



12-2016

Preliminary Study of Optical-Flow Based Background-Oriented Schlieren Measurements

Hassan A. Ghazwani

Western Michigan University, eng-alghazwani.hassan@hotmail.com

Follow this and additional works at: http://scholarworks.wmich.edu/masters_theses

Recommended Citation

Ghazwani, Hassan A., "Preliminary Study of Optical-Flow Based Background-Oriented Schlieren Measurements" (2016). *Master's Theses*. 762.

http://scholarworks.wmich.edu/masters_theses/762

This Masters Thesis-Open Access is brought to you for free and open access by the Graduate College at ScholarWorks at WMU. It has been accepted for inclusion in Master's Theses by an authorized administrator of ScholarWorks at WMU. For more information, please contact maira.bundza@wmich.edu.



PRELIMINARY STUDY OF OPTICAL-FLOW BASED BACKGROUND-ORIENTED
SCHLIEREN MEASUREMENTS

by

Hassan A. Ghazwani

A thesis submitted to the Graduate College
in partial fulfillment of the requirements
for the degree of Master of Science in Engineering (Mechanical)
Mechanical and Aerospace Engineering
Western Michigan University
December 2016

Thesis Committee:

Tianshu Liu, Ph.D., Chair
Christopher Cho, Ph.D.
Javier Montefort, Ph.D.

PRELIMINARY STUDY OF OPTICAL-FLOW BASED BACKGROUND-ORIENTED SCHLIEREN MEASUREMENTS

Hassan A. Ghazwani, M.S.E.

Western Michigan University, 2016

This research describes an experimental study on the density gradient by applying the Background Oriented Schlieren technique with the physics-based optical flow using a simple setup. The design of the BOS setup primarily consists of a background which has random dots, and a high-speed camera focused on the dots. Variation of the density between the undisturbed image and the disturbed image led to a shift of the dots, which is used to generate displacement field by using the optical flow method. In addition: different pressure conditions were applied, to provide distinct displacement fields. Finally, the density gradient of flow was visualized by BOS measurements based optical flow.

© 2016 Hassan A. Ghazwani

ACKNOWLEDGMENTS

First and foremost, I would like to express how thankful I am to my advisor Dr. Tianshu Liu, for his inspiration, tolerance, excellent guidance, unweaving confidence and support throughout this project. He has provided countless helpful suggestions and has pushed me to be my best. I am grateful to my committee member Dr. Christopher Cho for his assistance, confidence, and support on this project. Also, I express my gratitude to Dr. Javier Montefort for his assistance, confidence, and support on this project.

I wish to thank the government of Saudi Arabia and Jazan University who believed in me and provided me with a generous scholarship.

I would like to thank my wife, Sahar and my children Abdulmaieed and Abdulaziz, for their loving support and have provided me with strength and conviction to conclude this project. I am also very much obliged to my friend Hady who helped me by his suggestion and explanation through my project. Thanks for my friends, Alla attar, Patric, Jacob, Hadi Madkhali, Hassan Fagehi, Mofareh Ghazwani, and Chad Blackwell, for their unconditional support. Finally, I would like to thank my wonderful parents Ali and Kharifa for supporting me all throughout my educational studies. Their belief in my capacity to follow my dreams has guided me to achieve my goals education and it has made me who I am today. They are dearly missed.

Hassan A. Ghazwani

TABLE OF CONTENTS

ACKNOWLEDGMENTS	ii
LIST OF TABLES	v
LIST OF FIGURES	vi
LIST OF SYMBOLS	ix
1 INTRODUCTION	1
2 FLOW VISUALIZATION	3
2.1 Shadowgraph.....	3
2.1.1 Application of Shadowgraph Technique	7
2.2 Schlieren Technique.....	11
2.2.1 Application of Schlieren	14
2.3 Interferometry	18
2.4 Holographic Interferometry	19
2.5 Recent Imaging Technologies for Flow Visualization	21
3 LITERATURE REVIEW	22
4 BACKGROUND ORIENTED SCHLIEREN “BOS”	31
4.1 Geometrical Theory of Light Spread in Flow Field.....	31
4.1.1 The Gladstone –Dale Constant	33
4.2 Background Oriented Schlieren Theory	36

Table of Contents-Continued

4.3	BOS Measurements for an Inhomogeneous Density Field.....	39
4.4	Density Calculations	42
5	EXPERIMENTAL SETUP.....	44
5.1	Experimental Procedures and Measurements	44
5.2	Experimental Equipment	48
5.3	Data Processing.....	51
6	RESULTS AND DISCUSSION	54
6.1	Low Pressure.....	54
6.2	High Pressure	62
7	CONCLUSION AND FUTURE WORK	70
7.1	Conclusion	70
7.2	Future Work	71
	REFERENCES	72
	APPENDICES	
	A. Numerical Solution For Poisson Equation.....	74
	B. Matlab Code.....	76

LIST OF TABLES

4.1	Gladstone Dale constants for air [2]	34
4.2	Goldstone Dale constants for different gases [2]	35
5.1	Experimental equipment	48

LIST OF FIGURES

2.1	The general model of a shadowgraph system [2]	3
2.2	Deflection of light rays through glass (a) constant density field, (b) constant density gradient, (c) constant second derivative of density (d) variable second derivative of density [3].....	5
2.3	Shadowgraphs of bow shocks (a) Shadow formation by a bow shock (b) Bow shock around a sphere in $M=1.7$ flow [3]	6
2.4	Shadowgraph arrangement attached to T4 shock tunnel [4].....	8
2.5	Shadowgraphs at the intake of the scramjet (a) Combustion suppressed (fuel into nitrogen) (b) Fuel into air case [4].....	9
2.6	Shadowgraph images of the upstream section of the combustion chamber (a) with fuel but without combustion (b) with fuel and combustion [4].....	10
2.7	Schematic view of a typical schlieren imaging system [4].....	12
2.8	Horizontal knife-edge schlieren photograph of the flow field around a sphere at hypersonic speed [3].....	14
2.9	Schlieren setup through experiment [5].....	15
2.10	T-38 aircraft flying at Mach 1.1 [6]	17
2.11	Mach-Zehnder Interferometer [2]	18
2.12	Holographic interferometry layout [7].....	19
2.13	Flow left to right over flat plate [7]	20
3.1	Displacement field extract from a Eurocopter BK117 test [12]	23
3.2	Displacement fields extract from US helicopter test [12]	24
3.3	The average displacement field of density gradients vectors [13].....	25

List of Figures-Continued

3.4	Variation in refractive index field for Perspex rotated: (a) with clockwise and (b) anticlockwise [15].....	26
3.5	Average density gradient of Free jet (a) with control (b) without control [16]	27
3.6	Average density gradients of impinging jet (a) with control (b) without control [16]	28
3.7	The system setup for experimental [17].....	29
3.8	The pressure field for different resolution obtained by Optical flow-BOS and PIV-BOS [19]	30
4.1	Refraction of light ray through passing different flow field.....	32
4.2	Configuration of BOS system.....	37
5.1	The experimental setup for BOS.....	46
5.2	Photography of experimental setup	47
5.3	Flow chart of the density field calculation with BOS.....	53
6.1	The displacement magnitude fields for simple average of 500 images.....	55
6.2	Density field for simple average of 500 images at pressure 0.002 psi.....	56
6.3	Density field of random images. a- image no. 150, b- image no. 250, c- image no. 350, d- image no. 480.....	57
6.4	Density profile at different elevations.....	58
6.5	Normalizing density profile at different elevations	58
6.6	Overlapping density profiles at different elevations.....	59
6.7	Normalized overlapping density profiles at different elevations	60

List of Figures-Continued

6.8	Density fluctuation for sample average of 500 images.....	61
6.9	The displacement magnitude fields for sample average of 500 images.....	63
6.10	Density field for a sample average of 500 images at high pressure 0.005 psi.....	64
6.11	Density field of random images. a- image no. 150, b- image no. 250, c- image no. 350, d- image no. 480.....	65
6.12	Density profile for a sample average of 500 images at different elevations	66
6.13	Normalizing density profile for a sample average of 500 images at different elevations.....	66
6.14	Overlapping density profiles of a sample average from 500 images at different elevations	67
6.15	Normalized overlapping density profiles for a sample average of 500 images at different elevations.....	68
6.16	Density fluctuation for sample average of 500 images.....	69

LIST OF SYMBOLS

A	Distance Lens to field flow
D	Distance Background to field flow
Δy	Image displacement in y direction
f	Lens focal length
ε_y	Light deflection in y direction
M	Background image magnification
n	Refractive index
K	Gladstone-Dale constant
ρ	Density
C_0	The velocity of light in vacuum
C	The speed of light
Δx	Image displacement in x direction

X_{he}	Mole fraction of helium
K_{He}	Gladstone Dale constant for helium
K_{Air}	Gladstone Dale constant for air
ρ_{Air}	Density of air
ρ_{He}	Density of air
n_o	Refractive index of reference
W	The width of field test
R_e	Reynold number
μ	Fluid viscosity

CHAPTER 1

INTRODUCTION

A compressible flow field is investigated by using visualization methods. These methods depend on alterations in the fluid index of refraction of the flow. The methods give us the ability to analyze certain variables such as the gradients in the fluid density, temperature and static pressure. Through this method, one does not have to include the introduction of additives into the fluid. Three famous techniques: Shadowgraph, Schlieren and Interferometry. These techniques can be used for the measurement of density distribution. In many cases, flow visualization can be used with these techniques.

As widely known in the perspective of engineering, these methods can be adopted in many cases to the particular situation. Each technique is used to visualize flow field with specific density distribution. For example, the image that gives us the second derivative of density distribution can be visualized by using Shadowgraph while Schlieren is suitable for the first derivative density distribution. Also, an interferometry is the best to measure the density distribution with high resolution. Background Oriented Schlieren (BOS) is a well-known method to visualize density gradients in compressible flow.

The Background-Oriented Schlieren method originated from the classical Schlieren system. It was constructed under the name of synthetic Schlieren. The development of the digital camera and software processing have increased the efficiency of using BOS. Its setup is very simple: it consists of a background, which has random dots, and a camera to record high-resolution images of the background with and without the flow field between the two images. The processing of image pairs using optical flow coding by MATLAB to reveal small distortions of the background because of refractive disturbances in the flow field.

The flexibility of the BOS method allows for visualization of large-scale flow, including field test. One of the earliest outdoor applications of the BOS technique was the measurement of compressible blade-tip vortices created by helicopters in flight, imaged with backgrounds of concrete and grassy fields.

Investigating the density and variation in fluids by using BOS procedures has been applied increasingly over the last decades, due to recent improvements in technology, which have reduced the cost of electronics. Industry developments in camera imaging, lighting, and computer processing speed have all contributed to the rise of alternative techniques such as BOS. Flow visualization methods, such as Particle Image Velocimetry (PIV) and Planar Doppler Velocimetry (PDV), are currently being investigated in addition to BOS. Optical flow method and PIV are compared and explained comprehensively by Liu et al. in 2015 [1]. These methods depend on a laser to illuminate the fluid particles that are seeding to be visualized, while the BOS technique does not need the flow to be seeded for visualization.

CHAPTER 2

FLOW VISUALIZATION

2.1 Shadowgraph

The shadowgraph visualization procedure is a simple method to use when the density gradient of fluid flow is investigated. In the 1880's, Dvork analyzed this tool. Figure 2.1 shows a typical adjustment for the shadowgraph system. Alongside light rays are very important to apply the shadowgraph technique. The shadow is created on a vertical image due to the light rays that passed through the field under investigation. The shadow produced on a vertical image is recorded. To get better visualizing for the picture, the light source has to be small.

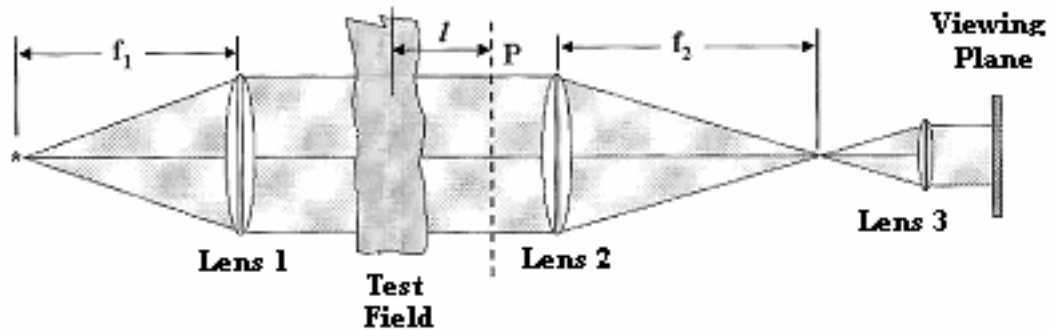


Figure 2.1: The general model of a shadowgraph system [2].

The blur in the image is given by ld^*f_1 , where f_1 is the lens or mirror focal length, d^* is the size of the source, and l is the distance of the observation plane from the optical disturbance region [2]. Most laboratory wind tunnels require the use of the second spherical and three lenses to reduce the size of the image. Lenses 2 and 3 are unnecessary for large scale visualization; however, a larger photographic plate is required to replace the large scale visualization so the picture will remain in full size.

The individual light rays have an angle of inclination from their original path due to the bending by refraction when light rays are passing through the field test. The shadowgraph is used to visualize the second derivative of the density gradient. Merzkirch [3] used a transparent plate of homogenous material to give simulate of refraction of light beams in density stratified. Through this experiment, he used glass plates, which have the same thickness, of different geometries. If the deflection of light beams in such way gives visible information about the flow, on the image plane, regions of differing light intensity could be determined. Also, non-uniform lighting would distinguish these areas.

The light rays were unaffected through passing the field has a constant density. Thus, the recording plane was consistently lit up as shown in Figure 2.2. The light rays were passing through a fluid field with $\frac{\partial n}{\partial y} = \text{const.}$ the recording plane was consistently lit up. The light rays were passing through fluid field with $\frac{\partial^2 n}{\partial y^2} = \text{const.}$ the bright for lighting was less but still uniform. The light rays were passing through a fluid field with $\frac{\partial^2 n}{\partial y^2} \neq \text{const.}$ the lighting was non uniform for the recording plane. Hence areas of shades of grey can be distinguished and flow information could be determined.

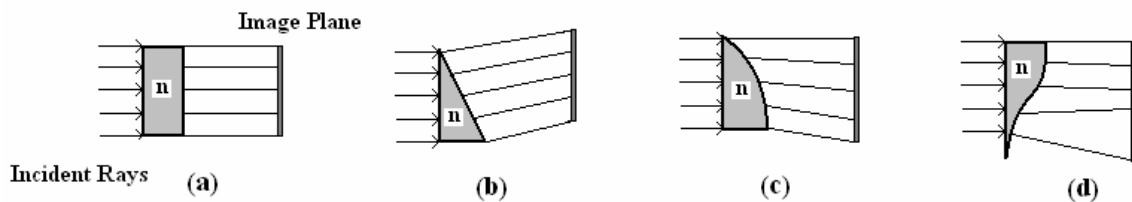


Figure 2.2: Deflection of light rays through glass (a) constant density field, (b) constant density gradient, (c) constant second derivative of density (d) variable second derivative of density [2].

In order to determine the density gradient, the intensity distribution in the image plane needs to be double integration, thus the shadowgraph is not appropriate for quantitative measurement. The grey shades are intensity distribution generally cannot estimated exactly for increasing errors introduced by the double of integration to be small.

Figure 2.3 demonstrates the light rays pass through a bow shock and noticed on the image plane were non-uniform. The light rays are deflected from their original paths and curve towards the intensive flow region downstream of the shock wave when the light beams pass the curved bow shock. This leads to create dark bands on the observation plane.

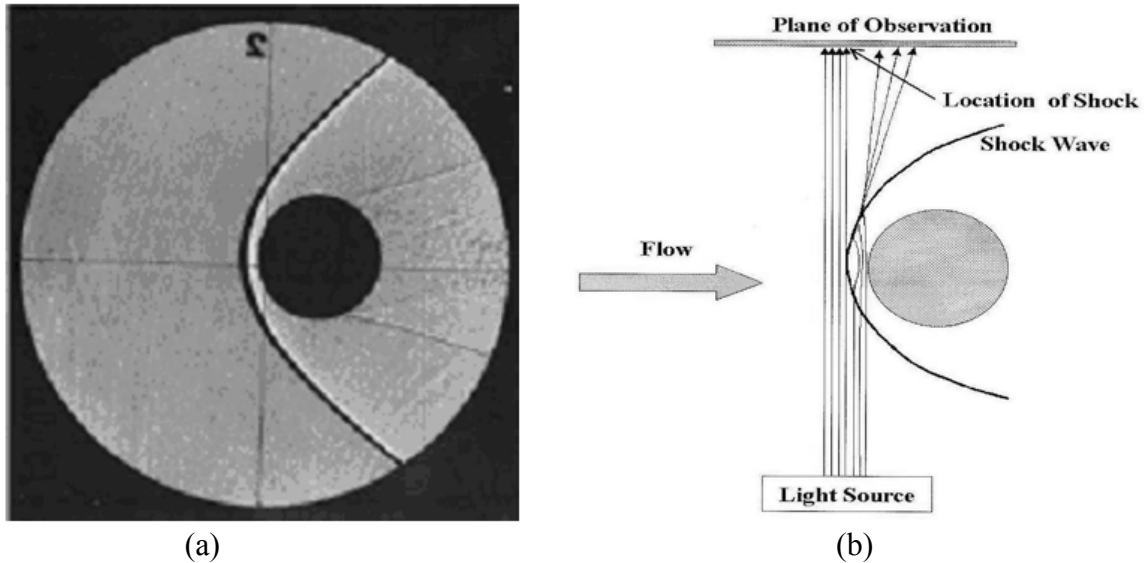


Figure 2.3: Shadowgraphs of bow shocks (a) Shadow formation by a bow shock (b) Bow shock around a sphere in $M = 1.7$ flow [3].

However, the shadowgraph is an appropriate for a quick investigation of flow fluids with density gradient. One application of shadowgraph for boundary layer and shockwave visualization are discussed next.

2.1.1 Application of Shadowgraph Technique

The shadowgraph technique was utilized to give proof of combustion in a supersonic ramjet engine. The shadowgraph technique was used through the experiment for studying the effect at the inlet injection in the combustion chamber and whether burning appeared in the combustion chamber.

Gardner [4] had made some change on the shadowgraph technique to be suitable for his work. Figure 2.4 shows the system that include a single pass adjustment was used to investigate the operation inside the T4 shock tunnel for the flow at intake two dimensions scramjet model. With 10 mm float glass sidewalls and a 250 μ s pulse from a ruby laser (694 nm) illuminated for these conditions the combustion chamber and scramjet intake were fitted. The objective for set up the laser system was to visualize the intake and the combustion chamber. The main goal was to investigate the reduction of viscous drag by shorting the length of the combustion chamber of a scramjet engine. In this case the fuel mixed upstream of the combustor because fuel was injected through portholes on the intake upstream of the combustion chamber.

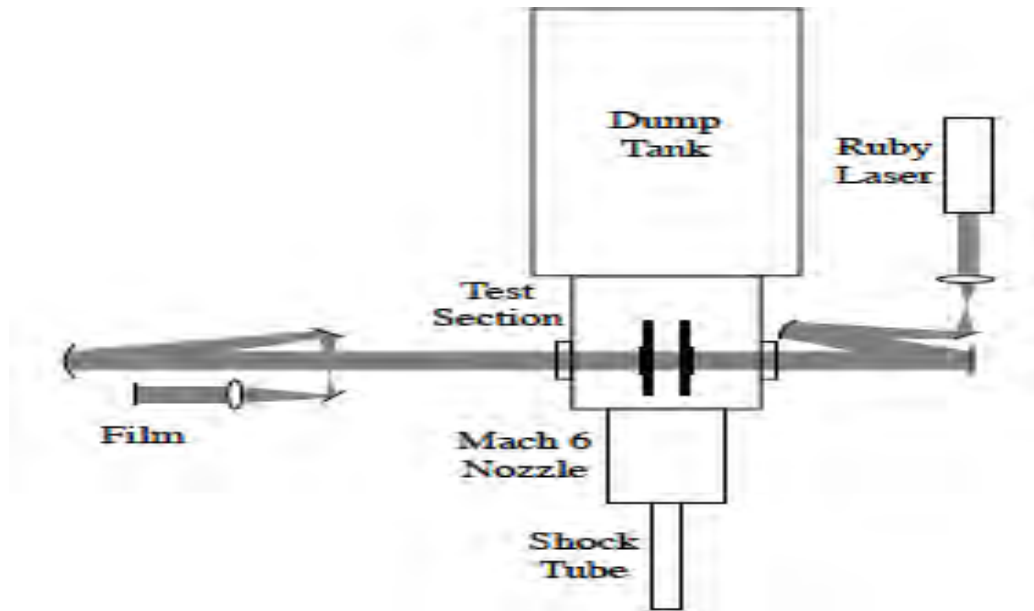


Figure 2.4: Shadowgraph arrangement attached to T4 shock tunnel [4].

The images of shadowgraph did not help to show evidence of in the intake of the scramjet model the combustion was occurring. Figure 2.1 (a) and (b) show the identical of shock angles for two cases where combustion was suppressed by injecting fuel into nitrogen and fuel into air. The shadowgraph demonstrated that for both cases the combustion chamber remained unshocked. This information was used to confirm that the inlet injection did not lead to chocking at that condition.



(a)



(b)

Figure 2.5: Shadowgraphs at the intake of the scramjet (a) Combustion suppressed (fuel into nitrogen) (b) Fuel into air case [4].

The following step of the experiment was to set up the shadowgraph system in order to visualize the flow in the combustion chamber of the model and to determine if the combustion occurred in the combustion chamber. Processing images of shadowgraph system had an evidence of burning happened in burner. Figure 2.6 presented two differences in chock positions were attributed to a change in Mach number because the released heat associated with the combustion of the fuel. This experiment has shown that the shadowgraph technique was beneficial tool for the flow analysis from the scramjet.



(a)



(b)

Figure 2.6: Shadowgraph images of the upstream section of the combustion chamber (a) with fuel but without combustion (b) with fuel and combustion [4].

2.2 Schlieren Technique

The Schlieren technique has created since two century by Toepler. It is used to visualize the light beams when passing through two different mediums. The gradients of density between two mediums have affected on the light rays to be deflected their paths from the original paths. This technique have reviewed and updated by Merzkirch [3] and Settles in 2001. The first application for the Schlieren system by Toepler was for visualization the compressible fluids. By setting the diameter of optical filed elements in the Schleren system is used to limit the flow field size. In addition, the Schlieren techniques generally give qualitative information of the density gradients in the flow.

Similar to shadowgraph, the Schlieren technique depends on the parallel or collimate light ray that passed through the test flow field. The method basically comprises of a point light source, either a laser or spark with a circular or slit aperture that is set at the focal length of lens 1 as illustrated in Figure 2.7. The light focuses on the image plane by the parallel light passes through the test field and lens 2. The intensity of light illuminating the photographic plate is reduced by the knife-edge, which is located at the focal plane of lens 2 and is positioned to cut off part of the light as seen on the image plane. The light beam is deflected by angle ϵ when passing through test field. The deflect angle ϵ lead to shift the distance Δs which is given by $\Delta s = f_2 \tan \epsilon$, where f_2 is the focal length of lens 2. The relative intensity change at the image is given by Merzkirch [3] and can be written as:

$$\frac{\Delta I}{I} = \frac{Kf_2}{s} \int_{\gamma_1}^{\gamma_2} \frac{1}{n} \frac{\partial n}{\partial y} dz, \quad (2.1)$$

where γ_1 and γ_2 are the z coordinates at which the light beam enters and leaves the test field and s is the reduced height of the light source image. As the ratio $(\frac{s}{f_2})$ decreases, the contrast on the photographic film increases [3].

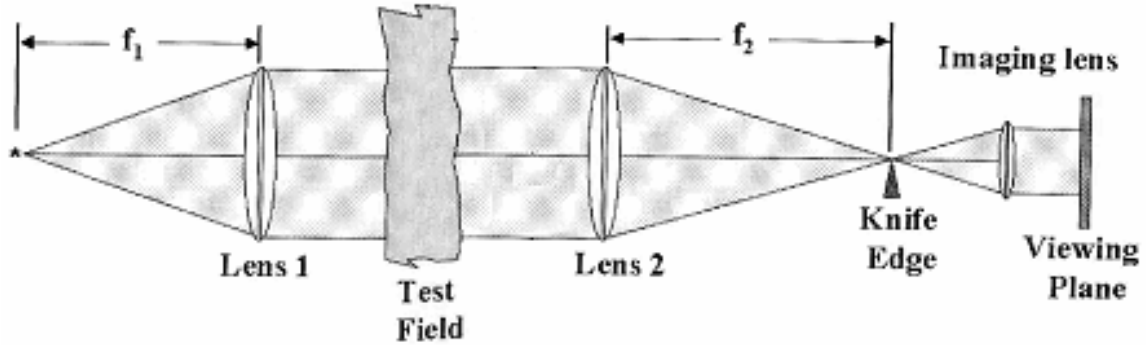


Figure 2.7: Schematic view of a typical Schlieren imaging system [2].

There are many ways to extract quantitative information from Schlieren images. The first way is a simple technique includes analyzing Schlieren curves of equal photographic density and is used for analyzing high-speed images, this technique is known as an isodensity tracer technique. Another technique of evaluating Schlieren images quantitatively was by integrating the distribution of the deflection angles to calculate the density distribution. However, the intensity at any point (x,y) on the image plane was affected by the characteristics of the photographic plate material and the developing process, that was a common problem that faced for Schlieren technique [3].

2.2.1 Application of Schlieren

Figure 2.8 demonstrates a case of a horizontal knife-edge schlieren photograph for the flow field around a sphere at hypersonic speed. The reverse in intensity levels as gradients change sign from top to bottom of the image lead to make the density gradients visible.

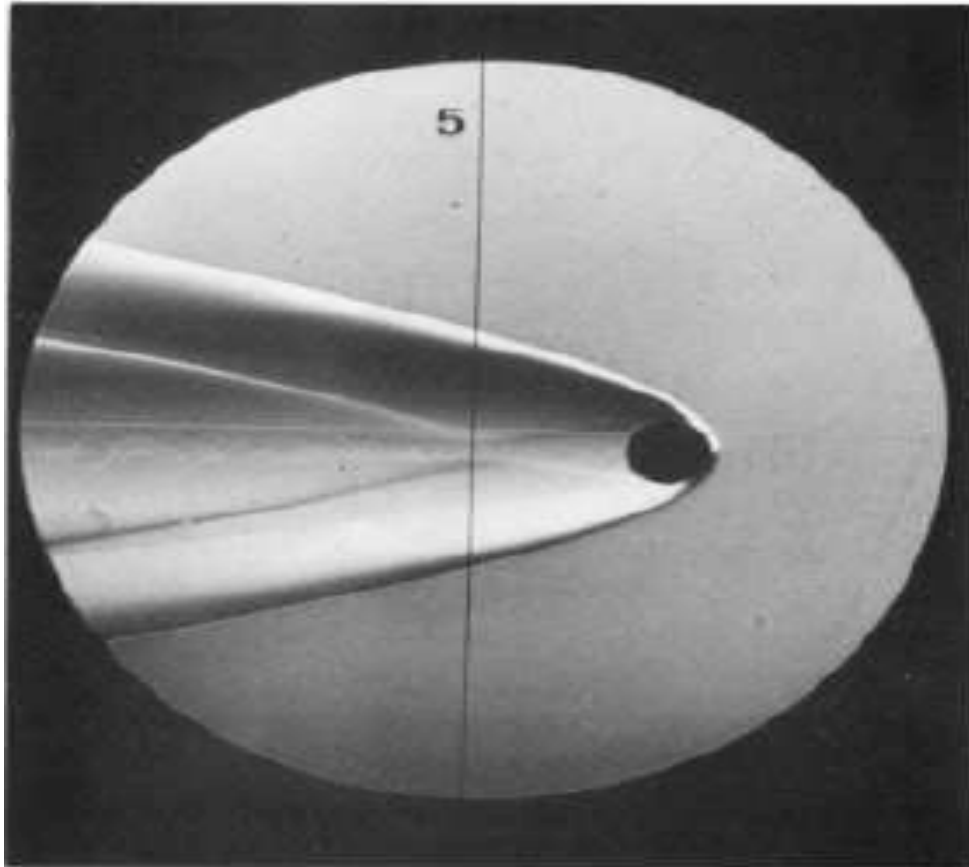


Figure 2.8: Horizontal knife-edge schlieren photograph of the flow field around a sphere at hypersonic speed [3].

In 2001, Lamar presented an example of Schlieren experiment for flow visualization in a supersonic wind tunnel. The system was setup in the wind tunnel to get a good visible for the flow field. Lamar's experiment was to investigate shock waves, which generated around a wind-tunnel model at the NASA Langley research Center in the Langley Unitary Plan Wind Tunnel (UPWT), by using a laser illumination and Schlieren imaging techniques. Figure 2.9 illustrates the setup for the experiment and the main components to build the system, which consists of a light source, two spherical mirrors, knife edge, optical beam splitter, still camera, flat mirror, video camera, and image screen [5].

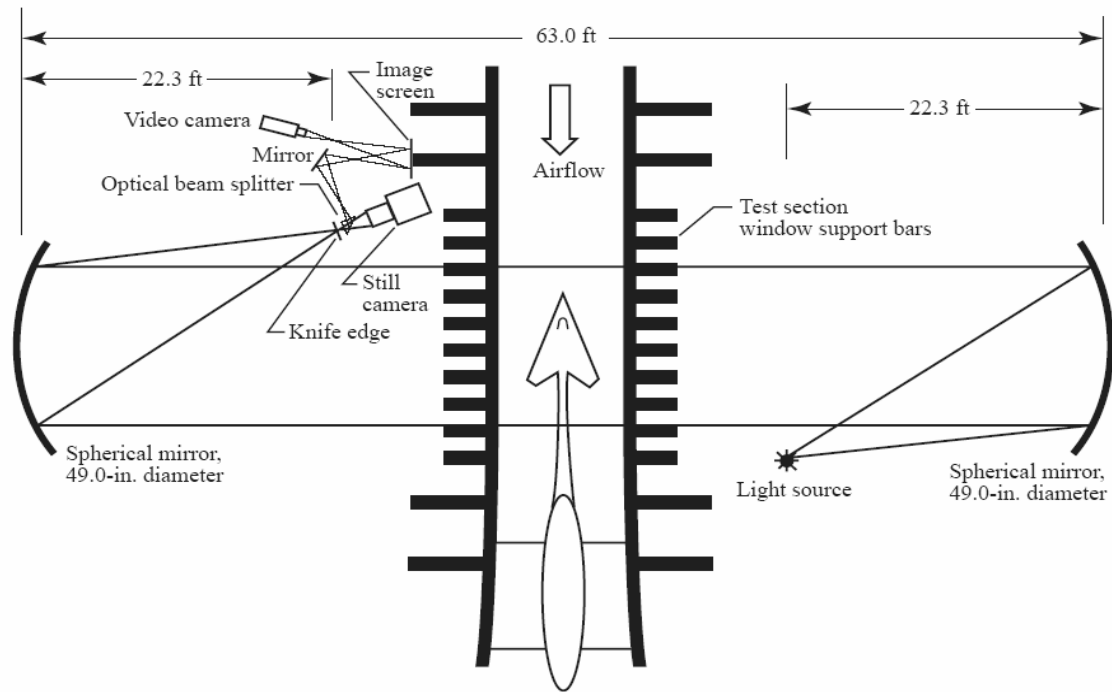


Figure 2.9: Schlieren setup through experiment [5].

Throughout the test, a 70 mm Hasselblad camera was used for still photographs. To extract useful information of the shock waves, the images were filtered and processed by using standard photographic software. Large plates were used in order to give high resolution for images. The consequence details of flow structures could be viewed by zooming on the regions of interest.

Another application of the Schlieren method was for large-scale flow under unusual illumination conditions [6]. Figure 2.10 presents the Schlieren technique was used to visualize shock wave structures that created around a T-38 aircraft flying at Mach 1.1 form NASA Langley Research Center to NASA Wallops test facility. The gross reflection was directly visible due to the change of density, which was considerable over the shock waves. However, the experiment was only successful with particular lighting and background conditions dependent on the humidity of air. The appropriate condition for visualization was rarely encountered. The main components for the experiment were a high-resolution telescope with focusing capabilities, which was focused on the sun, and a streak camera. In order to reduce the intensity of the sun to be suitable, a neutral filter was used.

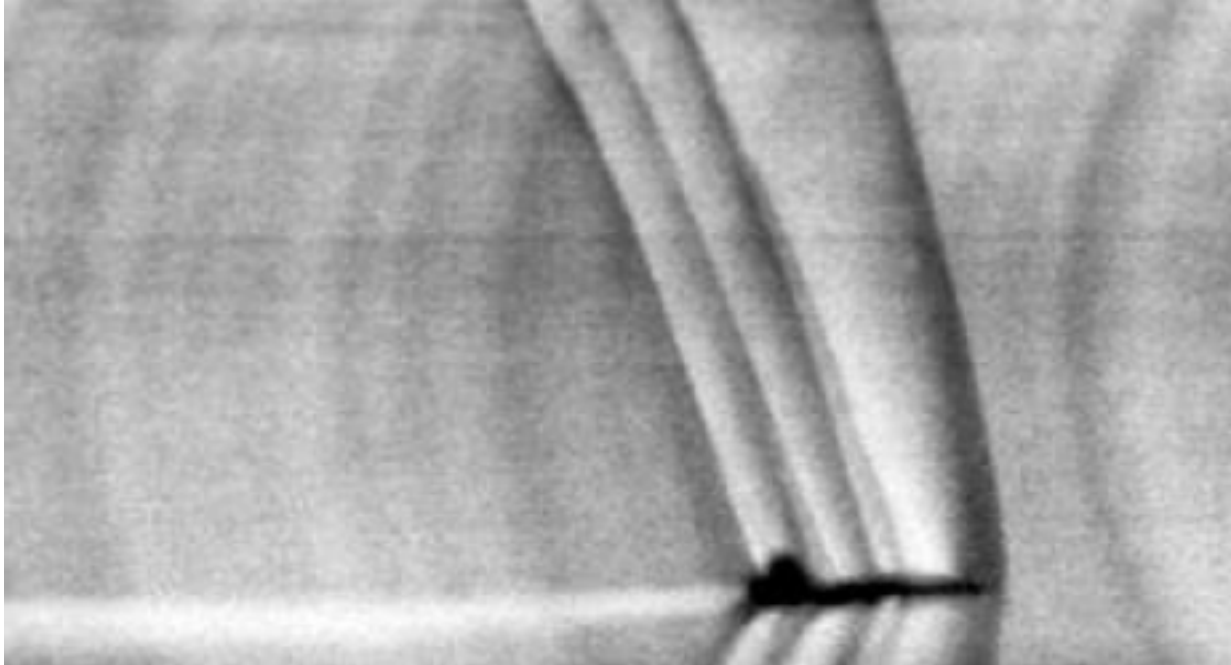


Figure 2.10: T-38 aircraft flying at Mach 1.1 [6].

2.3 Interferometry

The interferometry is a complicated technique for flow visualization in a compressible flow because it is used to visualize the density or refractive index directly without changing. The shadowgraph and Schlieren techniques depend on the light deflection for visualization while the interferometry method is used to extract information by evaluating the change of the beam phase.

The recent use of the interferometry technique was the Mach-Zehnder interferometry. The interferometer, as shown in Figure 2.11, consisted of a beam splitter, coherent light source, mirrors and a recording image system. The incident parallel rays separated by the beam splitter into a reference and an object beam. When a small intersection angle is presented between the two beams, Parallel fringes would show up on the image plan. Through the light beam passed a test field, the fringes appeared deformed on the picture plane.

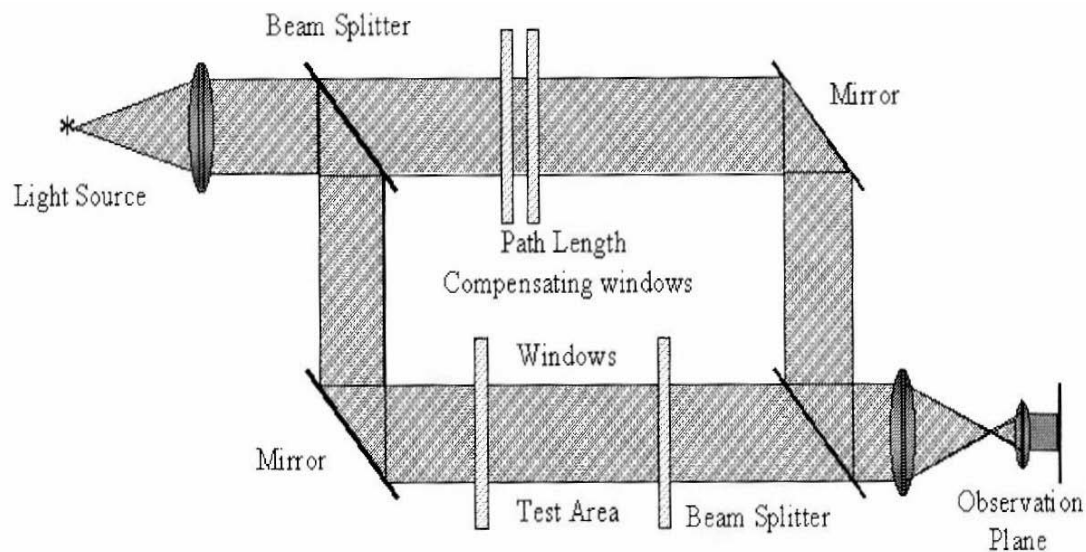


Figure 2.11: Mach-Zehnder Interferometer [2].

2.4 Holographic Interferometry

The main differences between the holographic interferometry and Mach-Zehnder interferometry are in the separation and the recombining for the light beams. In Mach-Zehnder the previous two light rays that are emitted at the same time are separated and recombined to interfere. In contrast, the holographic interferometry separation is temporal and the light beams are recombined to interfere at different times.

The Holography interferometry system shows in Figure 2.12 was used to study of the flow on the inlet of a scramjet engine. The experiment was conducted in the T4 reflected shock tunnel with a flat plate model at a slight angle of incidence to the free stream mounted in the test section.

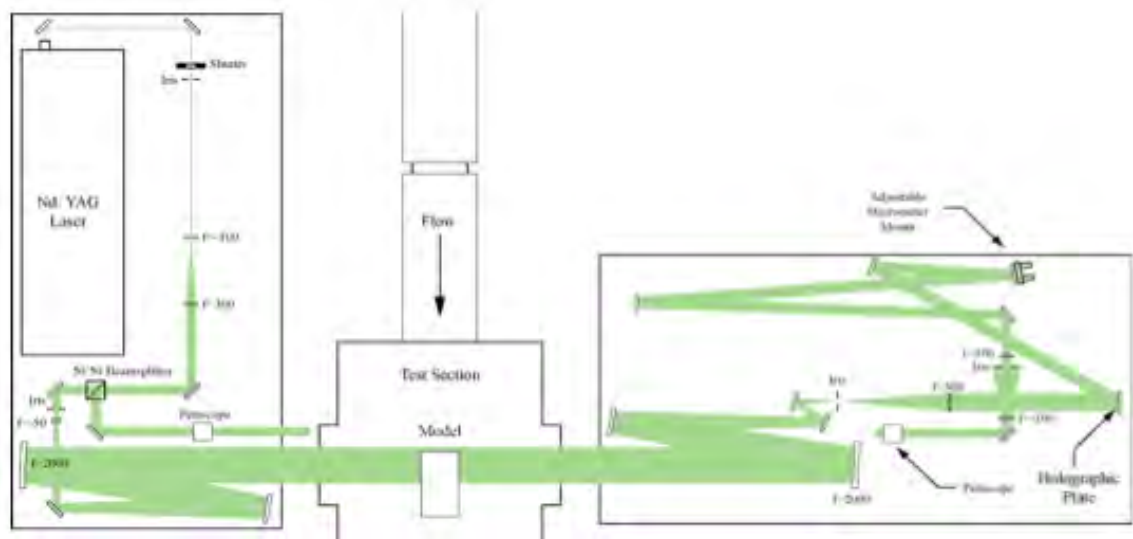


Figure 2.12: Holographic interferometry layout [7].

The light beam for the experiment was generated by laser of pulse width duration of 10 ns at 532 nm for the wavelength. The result that shown in Figure 2.13 illustrates the density changes connected with the shock waves and shear layers by the fringe shifts in the interferograms. Due to the shock wave from the tip of the flat plate, the edge shift is large at the top of the image. The injection of fuel into the flow is lead to a small bow shock.

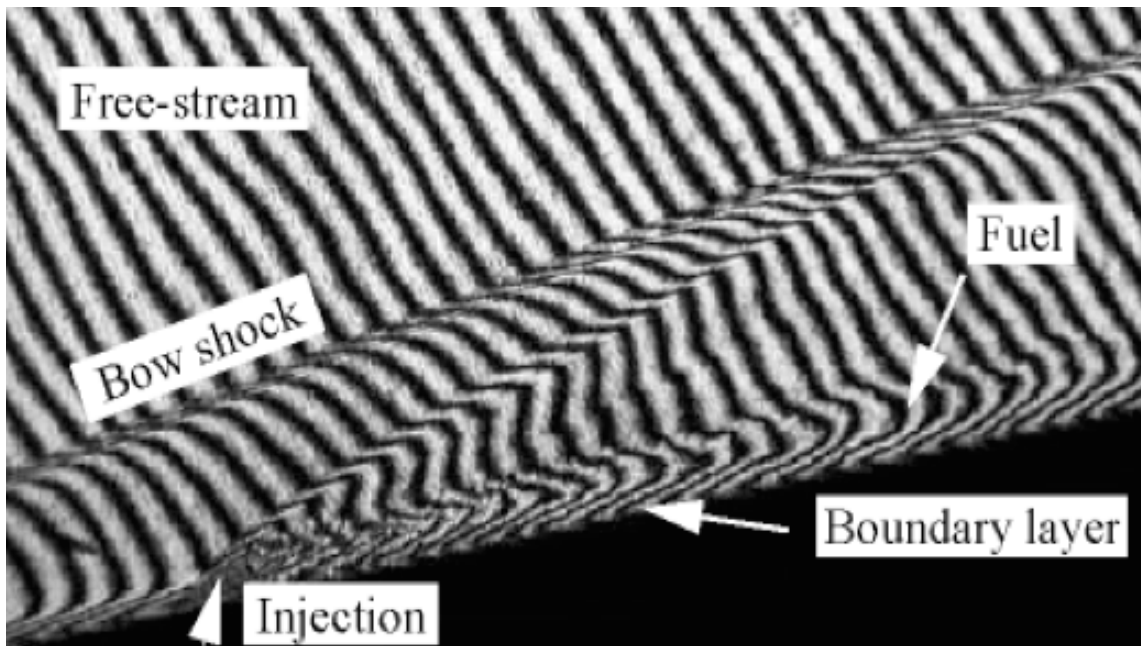


Figure 2.13: Flow left to right over flat plate [7].

2.5 Recent Imaging Technologies for Flow Visualization

The massive prosperity in the industrial of digital imaging cameras at relatively low cost has played a significant role to bring new techniques of non-intrusive flow visualization techniques. From measuring skin friction [8] to density measurements, different methods of flow visualization are being used. Meier [9] presented one of these techniques is Background Oriented Schlieren (BOS) technique. This method is used the same procedures that used in Particle Image Velocimetry (PIV) to extract flow information. In PIV, particles are added in flow for recording two images at a particular time interval. A laser or spark light is used to illuminate particles in order to take images by a CCD camera. These images contain information about the flow are extracted by using image processing method. The interest information of images recording is by how much particle are displaced between the two images. Also, the BOS system depends on the displacement between two images. The most common techniques for evaluating are cross correlation and optical flow.

In the compressible flow, variations in flow properties caused by gradual compression, in other regions dominated by viscous flow, in others regions due to the formation of shock waves around slender and blunted bodies. BOS technique has been introduced to visualize the flow using these density gradients.

CHAPTER 3

LITERATURE REVIEW

Many researchers have used the Background Oriented Schlieren (BOS) method to investigate and visualize the physical behavior of variables such as pressure, density, temperature and velocity. The BOS becomes widely used because it does not need sophisticated tools for setup. This chapter is shown the time period for the applications of the Background Oriented Schlieren (BOS) technique.

The first explanation for the Background Oriented Schlieren was under name “Synthetic schlieren” by Dealziel [10]. The Technique was invented to visualize the density gradient and to obtain quantitative information from whole field density measurement in two dimensions. It was used to study the density fluctuations of an internal wave field produced due to an oscillating cylinder. At the same period Raffel et al. [11] presented experiment for the possibility of applying the Background Oriented Schlieren for large scale. BOS technique was used to investigate unsteady density fields of blade tip vortices from a helicopter in hover flight. Density measurements were used to determine the pressure gradient, which producing by the rotating blade.

Richard and Raffel [12] illustrated the principle of Background Oriented Schlieren (BOS) technique by several applications. They studied the effect of the compressible vortices phenomenon on the blade vortex interaction. First investigation of the BOS method was applied for large scale to investigate vortices producing from two different subjects of helicopters “Eurocopter BK117 and US helicopter” with various backgrounds. The background for Eurocopter BK117 test was generated by splashing tiny droplets of white wall paint with a brush onto concrete ground while the grass of the airfield was used as background through the US helicopters test. Figure 3.1 shows the result of a Eurocopter BK117 test and demonstrates a young vortex shed from the blade and also the vortices that produced by previous blades. Figure 3.2 explains the displacement result of the US helicopter test. This displacement is due to the interaction between the blade tip vortices and the exhaust plume, which produced by the engine turbine.

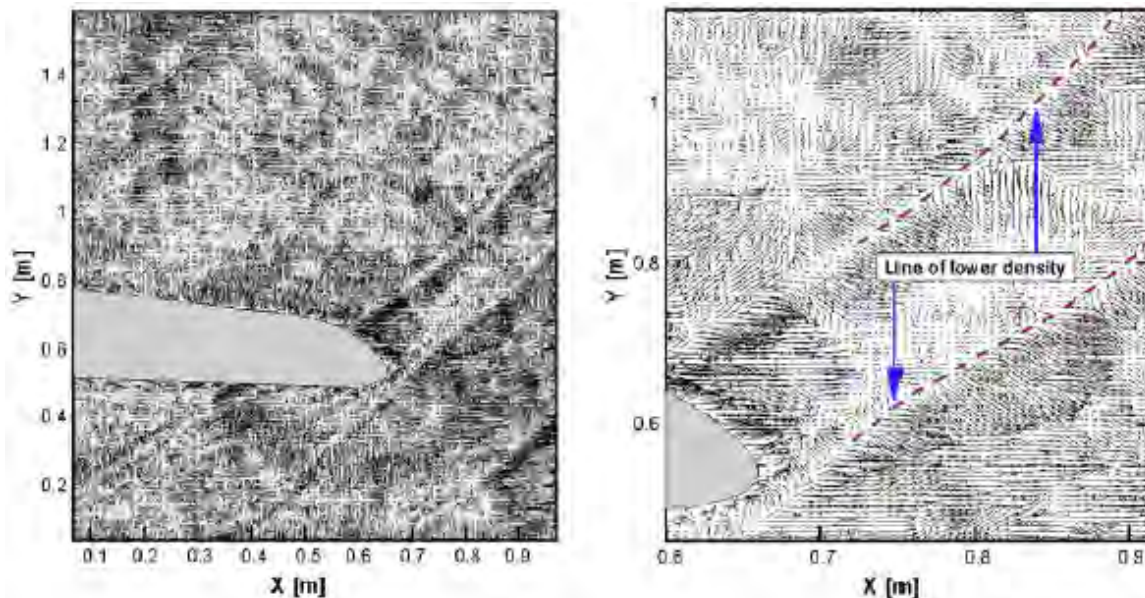


Figure 3.1: Displacement field extract from a Eurocopter BK117 test [12].

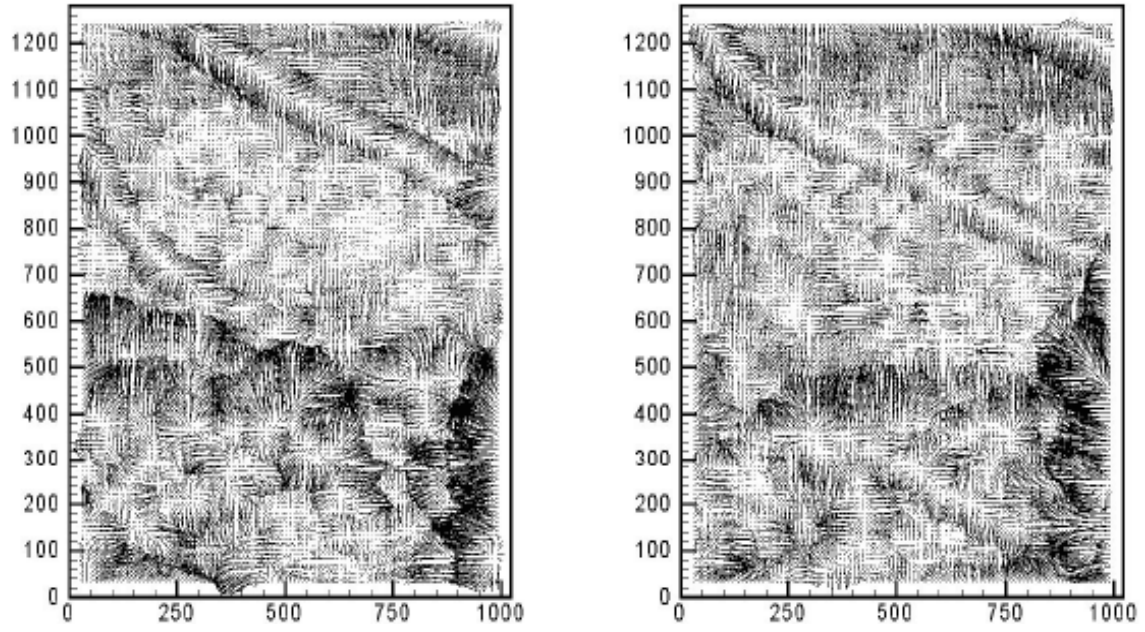


Figure 3.2: Displacement fields extract from US helicopter test [12].

Venkatkrishnan and Meier [13] applied BOS method on a cone cylinder with 15° (semi-apex angle) and flow at a Mach equals 2.0 in order to visualize the density field. The main purpose of these conditions is to validate BOS results versus cone charts [14]. The information of the BOS images was extracted by using a cross correlation algorithm and a Gaussian sub-pixel interpolation method. Figure 3.3 shows the vectors of image displacement for a cone cylinder at Mach equals 2. The result presents the forebody shock wave, which can be determined due to the displacement between the surface and the shock.

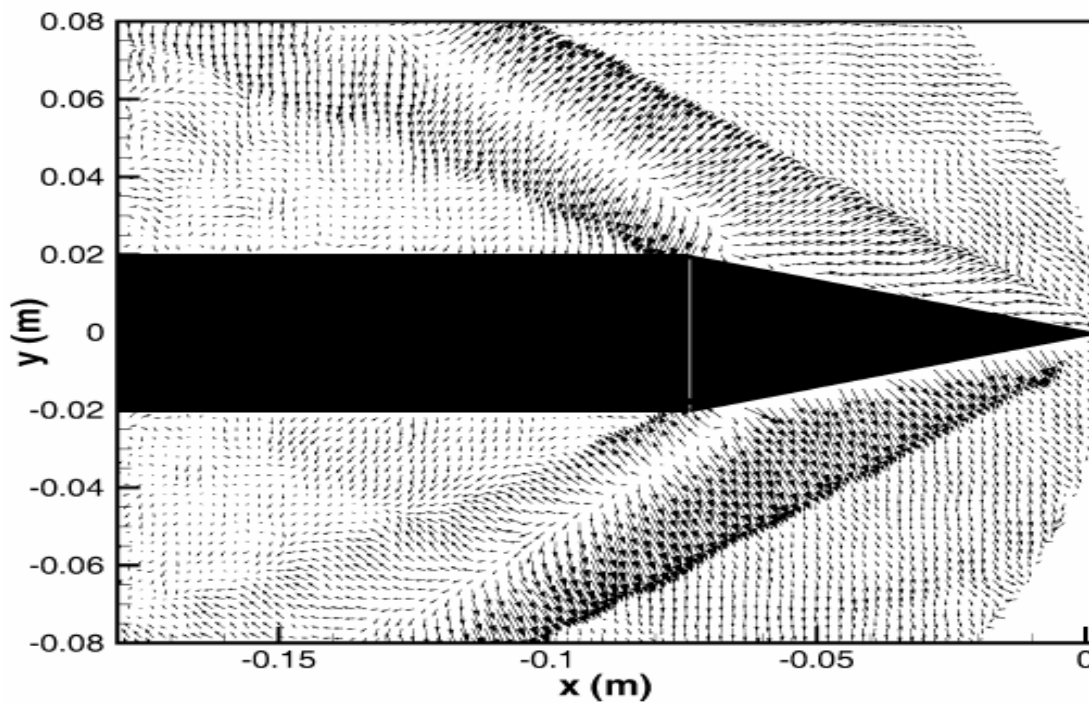
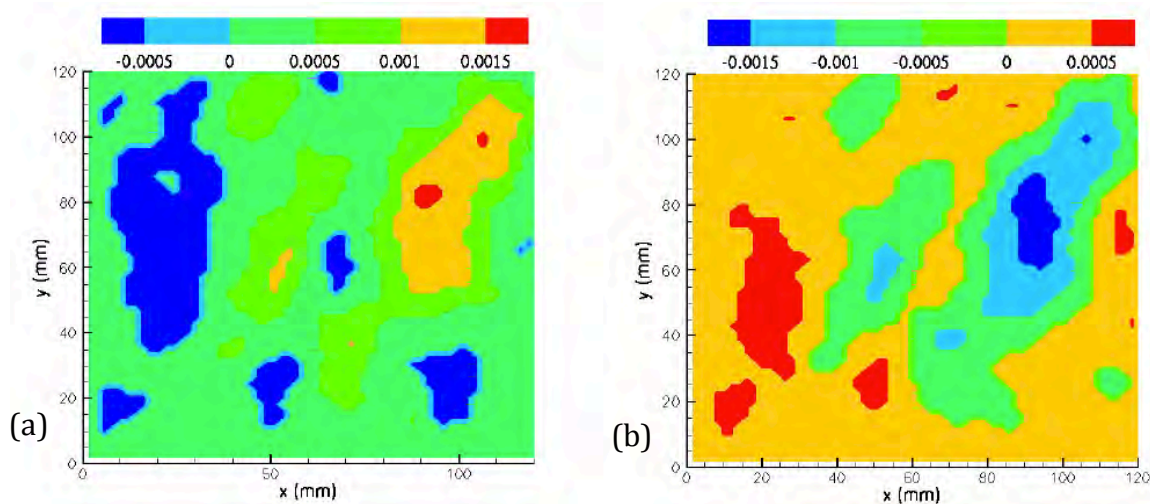


Figure 3.3: The average displacement field of density gradients vectors [13].

Vasudeva et al. [15] used the BOS method to measure the density distribution of a heated air jet. The Perspex was used through the experiment with particular characteristics of refractive index equals 1.495, length 140 mm and thickness 24.92 mm. The Perspex was perpendicular to the direction of light beams with rotating 5° with clockwise and anticlockwise through the test.



The effect of rotating the Perspex on the refractive index is shown in figure 3.4 for both stages.

Figure 3.4: Variation in refractive index field for Perspex rotated: (a) with clockwise and (b) anticlockwise [15].

Venkatakrishnan et al. [16] illustrated another application of BOS technique on a supersonic free and impinging jet. Micro jet was used for free jet and impinging jet in order to inspect its effect on the density field. A system was setup in the STOVL supersonic jet facility of the AAPL located at the Florida state university in Tallahassee. Aluminum plate was used as impinging surface and is located directly under the nozzle exit to receive the effect of the flow. The experiment was done by two cases (with control and no control) apply on free jet and impinging jet. Comparison between the results of free jet for two cases, there were significantly different in the density gradients as shown in figure 3.5. In the case with control the jet appear steady and the shock structures were weak. Also, for both cases for impinging jet the fluctuation of density was different and the mild shocks had vanished as presented in figure 3.6.

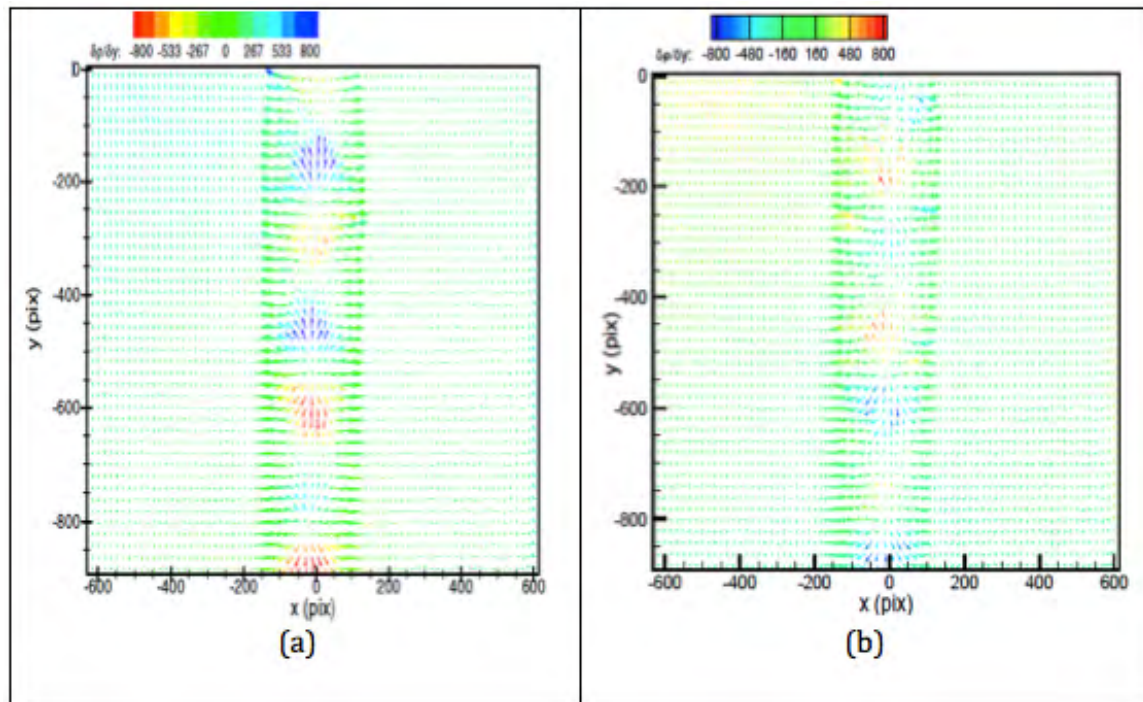


Figure 3.5: Average density gradient of free jet (a) with control (b) without control [16].

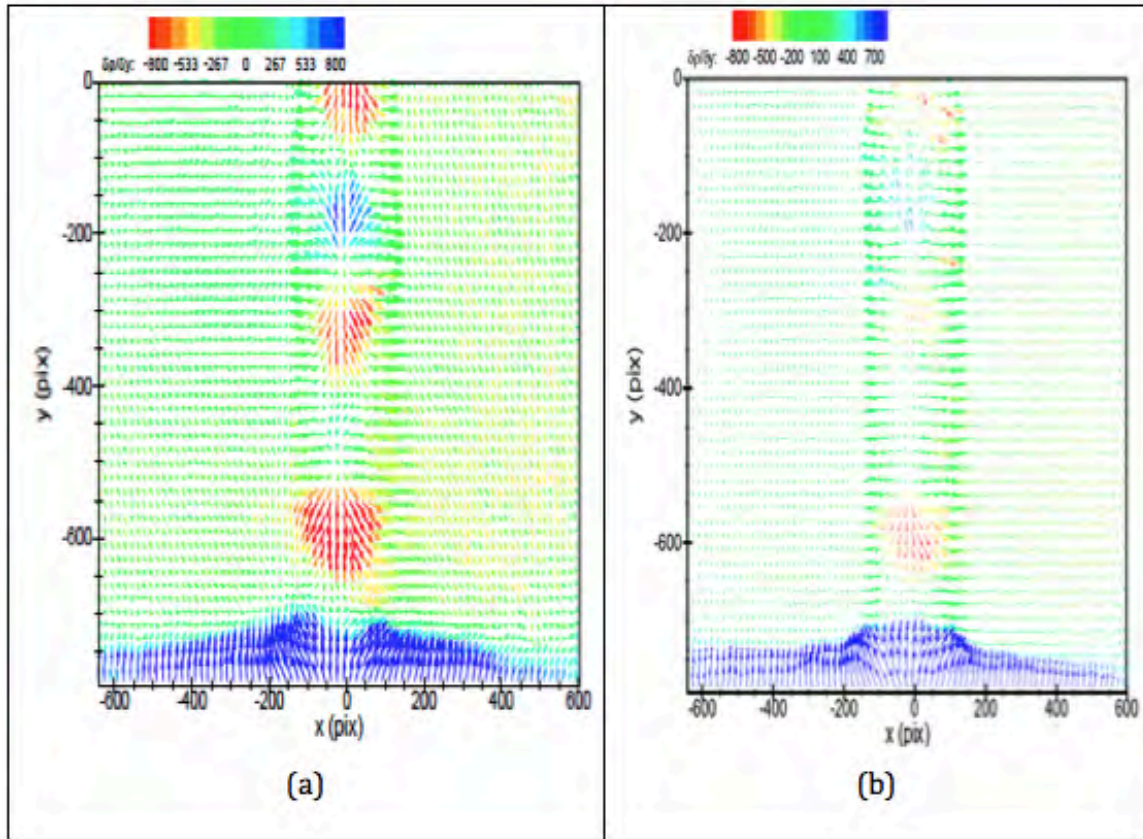


Figure 3.6: Average density gradients of impinging jet (a) with control (b) without control [16].

The BOS technique is not applied just for measuring the density gradient. It can be used to determine the temperature field as Vinnichenko et al. [17] presented. The BOS method was combined with Infrared thermal imaging (IRTI) to measure the temperature field within liquid layer below the liquid and gas interface. The kind of liquid and gas are respectively water and ethanol. The system was setup as shown in the figure 3.7. Furthermore, Kotchourk et al. [18] explained the possibility of using BOS technique to determine the concentration measurements of a round hydrogen jet. The system was setup to make the flow vertical in order to study the free expanding vertical axisymmetric hydrogen jets. The visualization for concentration gradient and concentration itself was investigated using BOS system. Under investigation the hydrogen jets had a nozzle diameter of 21 mm and constant flow rate equal to 3 g/s.

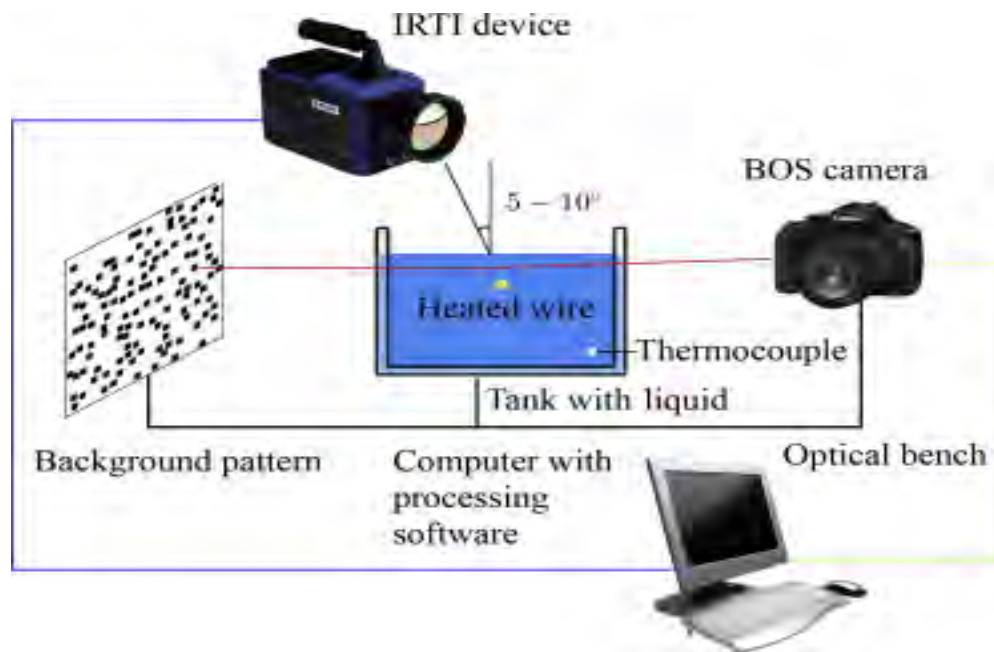


Figure 3.7: The system setup for experiment [17].

The newest application of BOS technique was presented by Hayasaka et al. [19]. They explained the possibility of BOS system to extract information of density gradients in tiny sizes of scales. The BOS method was used to investigate the shock wave, which produced underwater by a laser, by identifying the displacement vectors of local density gradients of water in order to obtain the pressure field. However, this experimental presented the benefit of the Optical flow comparing with PIV (cross correlation) in terms of the resolution. Figure 3.8 shows the difference of the pressure field obtained by Optical flow and PIV. The Optical flow can deal with high resolution lead to detect a lot of vectors is capable of measuring shock wave under water.

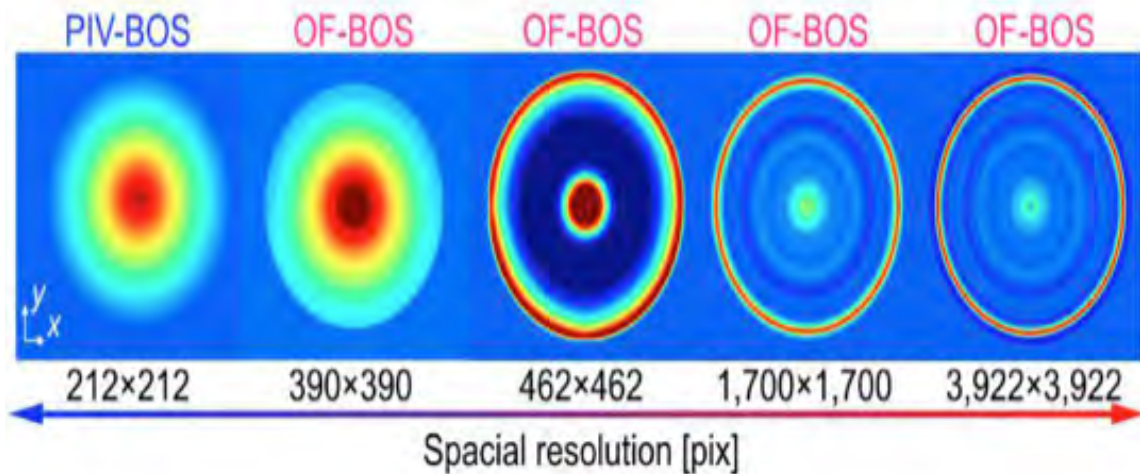


Figure 3.8: The pressure field for different resolution obtained by Optical flow-BOS and PIV-BOS [19].

CHAPTER 4

BACKGROUND ORIENTED SCHLIEREN “BOS”

The light is played crucial role in studying the flow field by visualization. The physical characteristics for the light are giving intensive information when passing through different mediums of the fluid. The light is imperative for the Background Oriented Schlieren to work. The basis physical for the BOS system is derived from Snell’s Law, explains the light behavior which is affected with matter.

4.1 Geometrical Theory of Light Spread in Flow Field

The speed of light propagates by the electromagnetic waves, and the higher density leads to resistance for the electromagnetic waves. The density of the fluid is measured by molecule per unit volume. The refraction of index n is the proportional of the peace of light in a vacuum and the rate of light in the flow field, and is not constant for all fluid. When the light transmits through inhomogeneous mediums of refractive index that lead to refract the light from its original path. Figure 4.1 presents the geometry of light deflection through passing different fields of index of refraction.

$$n = \frac{C_0}{C} \quad (4.1)$$

Where n : is the index of refraction. C_0 is the speed of light in vacuum and C is the velocity of light as a component of medium.

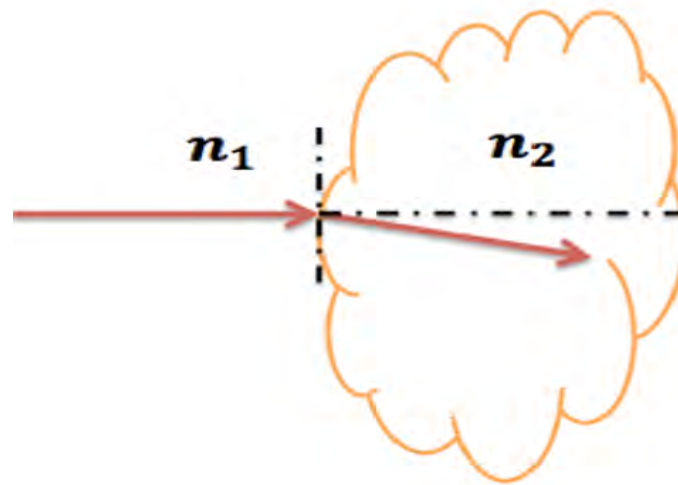


Figure 4.1: Refraction of light ray through passing different flow field.

In compressible flows the change in density occur fast and massive. Beams of light are refracted by the difference distribution of the refractive index through passing regions of density gradients. The light deflection in these regions are occurred in two ways. First, the original path of the light is deflected; second, the disturbed phase of the light wave is shifted respect to that of an undisturbed light beam. Performing quantitatively of the density measurements and visualizing the flow field qualitatively are based on these phenomena. The next point will discuss is the Gladstone Dale, which explains the relation between the density fluid and its refractive index.

4.1.1 The Gladstone –Dale Constant

The Gladstone Dale constant [3] is the relation that connects the index of refraction of the fluid to its density. This constant based on the characteristics of the gas in the field and on the wavelength of light used. The Gladstone Dale equation is simplified and derived from Lorentz-Lorenz equation [20] and is expressed as:

$$n = 1 + K\rho \quad (4.2)$$

where K is the Gladstone Dale constant and ρ is the density of test field. For a gas such as air which is a mixture of several gases the Gladstone Dale equation form is expressed as:

$$n = 1 + \sum_i K_i \rho_i \quad (4.3)$$

where K_i and ρ_i are the Gladstone Dale constants and the densities of the individual components. Tables 1 and 2 are respectively provides Gladstone Dale constants for air at 288 K and for various gases.

Table 4.1: Gladstone Dale constants for air [2].

K (m ³ /kg)	Wavelength λ (μm)
0.2239	0.9125
0.2255	0.6440
0.2264	0.5677
0.2281	0.4801
0.2304	0.4079

Table 4.2: Goldstone Dale constants for different gases [2].

Gas	K (m ³ /kg)
O ₂	0.190
N ₂	0.238
He	0.196
CO ₂	0.229

4.2 Background Oriented Schlieren Theory

The relation between the refractive index of the fluid and its density is the intrinsic principle to work the Background Oriented Schlieren (BOS) technique. This relation is illustrated by the Gladstone Dale equation. The BOS method is similar to the laser speckle density photography as described by Deburs et al. and Köpf and then improved by Merzkirch [20]. The laser speckle density photography is measured the refractive deflection of rays in a light beam that passing through a flow with varying refractive index or fluid density. However, as opposed to other interferometry, laser speckle models are created rather than interference borders. The BOS technique has advantage comparing with the quantitative optical techniques because it simplifies for recording. The speckle pattern, usually produced by the expanded laserbeam and ground glass, is replaced by a pattern on a surface in the background of the test volume. This pattern, which consists of small dots distributed randomly, has to have a high spacial frequency that can be imaged with high contrast [12].

The BOS system needs for using two images. First image is taking without flow by observed the background pattern through air and called image reference. The second image exposures with flow that result into displacement in the random dots of background pattern. Both images can be processing by using some correlation methods or optical flow. These algorithms are written by using some programing language such as MATLAB, which used to determine the displacement between the random dots of the background pattern at different locations.

Figure 29 illustrates the configuration of BOS technique that based on the deflection of light beams. Each single beam deviation has information about the variation of the refractive index integrated over the line of sight.

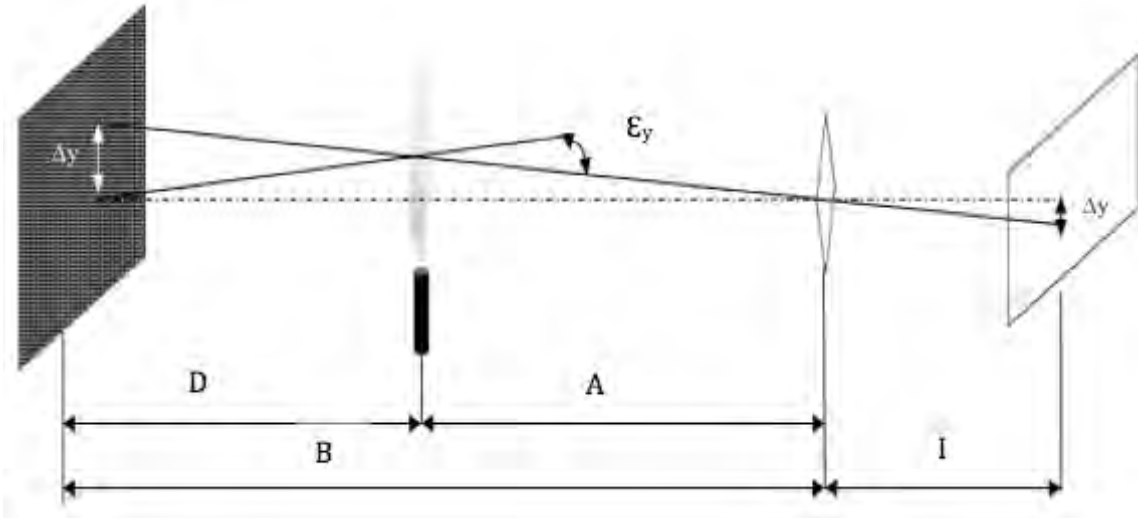


Figure 4.2: Configuration of BOS system.

The image displacement Δy for the BOS technique, can be derived by assuming a small deviation angles [20].

$$\Delta y = DM\varepsilon_y, \quad (4.4)$$

where $M = \frac{1}{B}$, is the magnification factor of the background and D is the distance between the dot pattern and the inhomogeneous density and the deflection angle

$$\varepsilon_y = \frac{1}{n_o} \int \frac{\partial n}{\partial y} dz, \quad (4.5)$$

So, the image displacement can be rewritten as:

$$\Delta y = f \left(\frac{D}{D + A - f} \right) \varepsilon_y. \quad (4.6)$$

A is the distance between the lens and the flow field and the focal length of the lens f . For a large distance between the background and the object field, (D), and the object become close to the lens that means a small A , the equation 4.6 shows the large image displacement can be obtained for those conditions.

4.3 BOS Measurements for an Inhomogeneous Density Field

Fermat's principal is explained the behavior of light in an inhomogeneous field travelling between two points. The principle is defined as:

$$\delta \int n(x, y, z) ds = 0 , \quad (4.7)$$

where $n(x, y, z)$ is the index of refraction and s denotes the arc length over the light beam. The equation is simplified in terms of the light ray parallel to the z -axis. It can be formed by the differential equations as follows:

$$\frac{d^2x}{dz^2} = \left[1 + \left(\frac{dx}{dz} \right)^2 + \left(\frac{dy}{dz} \right)^2 \right] \left[\frac{1}{n} \frac{\partial n}{\partial x} - \frac{dx}{dz} \frac{1}{n} \frac{\partial n}{\partial z} \right], \quad (4.8)$$

$$\frac{d^2y}{dz^2} = \left[1 + \left(\frac{dx}{dz} \right)^2 + \left(\frac{dy}{dz} \right)^2 \right] \left[\frac{1}{n} \frac{\partial n}{\partial y} - \frac{dy}{dz} \frac{1}{n} \frac{\partial n}{\partial z} \right], \quad (4.9)$$

These equations describe the path of light through inhomogeneous field as presented in figure 4.2. The light ray travels in the z-direction and the image views plane in the x-y plane. In a compressible flow the deviation in the z-direction is very small, that leads to the assumption for the slopes $\frac{dx}{dz}$ and $\frac{dy}{dz}$ are insignificant [3]. The equation is reduced to

$$\frac{d^2x}{dz^2} = \frac{1}{n} \frac{\partial n}{\partial x}, \quad (4.10)$$

$$\frac{d^2y}{dz^2} = \frac{1}{n} \frac{\partial n}{\partial y}, \quad (4.11)$$

The tangent of the angle deflection ε of the light beam for the x and y direction is determined by integrating this set of equations. We obtain:

$$\tan \varepsilon_x = \frac{d^2x}{dz^2} = \int \frac{1}{n} \frac{\partial n}{\partial x} dz. \quad (4.12)$$

$$\tan \varepsilon_y = \frac{d^2y}{dz^2} = \int \frac{1}{n} \frac{\partial n}{\partial y} dz. \quad (4.13)$$

By back tracing the light beams received by camera [10], the apparent shift (Δx , Δy) in the origin of the light beams can be formed as

$$\Delta y = W(W + 2D) \frac{1}{n_o} \frac{\partial n}{\partial y} , \quad (4.14)$$

$$\Delta x = W(W + 2D) \frac{1}{n_o} \frac{\partial n}{\partial x} . \quad (4.15)$$

W is the width of the homogenous field and D is the distance between the background and test field.

The general solution for 2-D of whole field in terms of the refractive index gradient becomes as Poisson equation:

$$\frac{\partial^2 n}{\partial x^2} + \frac{\partial^2 n}{\partial y^2} = S(x, y) \text{ or } \nabla^2 n = S(x, y) , \quad (4.16)$$

$$S(x, y) = C \left[\frac{\partial}{\partial x} \Delta x(x, y) + \frac{\partial}{\partial y} \Delta y(x, y) \right] . \quad (4.17)$$

4.4 Density Calculations

In this work the main object is to observe and describe the density gradient of mixing helium gas and air. The density field can be obtained from Gladstone Dale equation for a helium-air mixture [3].

$$n - 1 = K_{He} \rho_{He} + K_{air} \rho_{air} = K_{He} X_{He} \rho_{oHe} + K_{air} (1 - X_{He}) \rho_{oair} . \quad 3)$$

Where ρ_{He} and ρ_{Air} are the partial densities for helium and air. X_{He} is the helium mole fraction. ρ_{oAir} and ρ_{oHe} are pure air and pure helium densities at the specific conditions from pressure and temperature (25 °C and 1 atm). K_{He} and K_{air} are the Gladstone Dale constants for both gases, which can be found in Table 4.2.

$$X_{He} = \frac{(n - 1) - K_{air} \rho_{air}}{(K_{He} \rho_{oHe} - K_{air} \rho_{air})}, \quad (4.19)$$

It is known that:

$$n_{air} - 1 = K_{Air} \rho_{oAir} . \quad (4.20)$$

Consequently:

$$X_{He} = \frac{n - n_{Air}}{(K_{He} \rho_{oHe} - K_{Air} \rho_{oAir})}. \quad (4.20)$$

So, it can be obtained the density field after once the helium friction is calculated.

$$\rho = X_{\text{He}}\rho_{\text{oHe}} + (1 - X_{\text{He}})\rho_{\text{oAir}} . \quad (4.21)$$

CHAPTER 5

EXPERIMENTAL SETUP

The experimental of the Background Oriented Schlieren method is conducted to investigate the physical parameters such as Pressure, Temperature and Density. The observation for gradients of those variables is very important in fluid mechanics. It is help to know the physical behavior for which variables by visualization under specific circumstances.

5.1 Experimental Procedures and Measurements

The experimental setup is comprised of a nozzle, digital camera, a tank of helium gas with pressure gauge, and the table on which the equipment was installed. The individual components were secured to the table as to reduce variations in measure. The nozzle, used throughout the experiment, has a 5.8 mm exit. This was screwed to a rectangular wood plate, which was in turn clamped to the table. The exit nozzle was checked to be vertical with a torpedo level. The pressure gauge was connected to the tank, which was connected to the nozzle with plastic tubing and sealed shut with hose clamps on both ends.

Furthermore, the camera, a Basler avA 1000-100 gm, was secured on a standard optical-grade breadboard, and positioned so that the nozzle was in the middle of its field of view. So that the camera would have enough exposure to capture 100 fps, two spotlights were placed symmetrically behind the camera as to light the background without shadow. The software used to fine-tune the camera was Pylon Viewer. The background used throughout the experiment was a sheet of cloth with dots randomly patterned on its surface. It was fixed by the corners with pins to a wooden frame, behind the nozzle relative to the camera.

To conduct the experiment, the lights were turned on, and the distances between the background and nozzle, and nozzle and camera were measured. The distance from the background to the nozzle was found to be 285.75 mm; the distance from the background to the camera was found to be 965.2 mm. The exit pressure was then measured for two cases- high pressure and low pressure. A Pitot tube (Manometer) was used to measure the exit pressure of the nozzle, the end of the tube vertically above the nozzle to accurately measure the flow. The high pressure was found to be 0.005 psi with Reynold number equal to 1007.96, and the low pressure was found to be 0.002 psi with Reynold number equal to 637.669. Using these pressures, the velocity can be calculated using following equation.

$$V = \sqrt{2 \frac{\Delta p}{\rho}} . \quad (5.1)$$

The Reynold number is calculated based on the diameter using following equation:

$$R_e = \frac{\rho V D}{\mu} , \quad (5.2)$$

where ρ is the density of helium, D is the diameter of nozzle, V is the velocity for flow field form the nozzle and μ is the viscosity of the fluid flow through the nozzle.

Finally, the camera captured one background image without helium flow, to use for reference, and 500 trial images with flow were captured. After taking these images, the optical flow code was used to analyze the images to extract the displacement, which is due to the variation of density, between two images, the reference and each of the trial images.

The BOS experimental as shown in Fig. 5.1 is illustrated the main components for the setup. It is composed of Camera, Nozzle, Background, Pressure Gauge and Tank reservoir of helium gas.

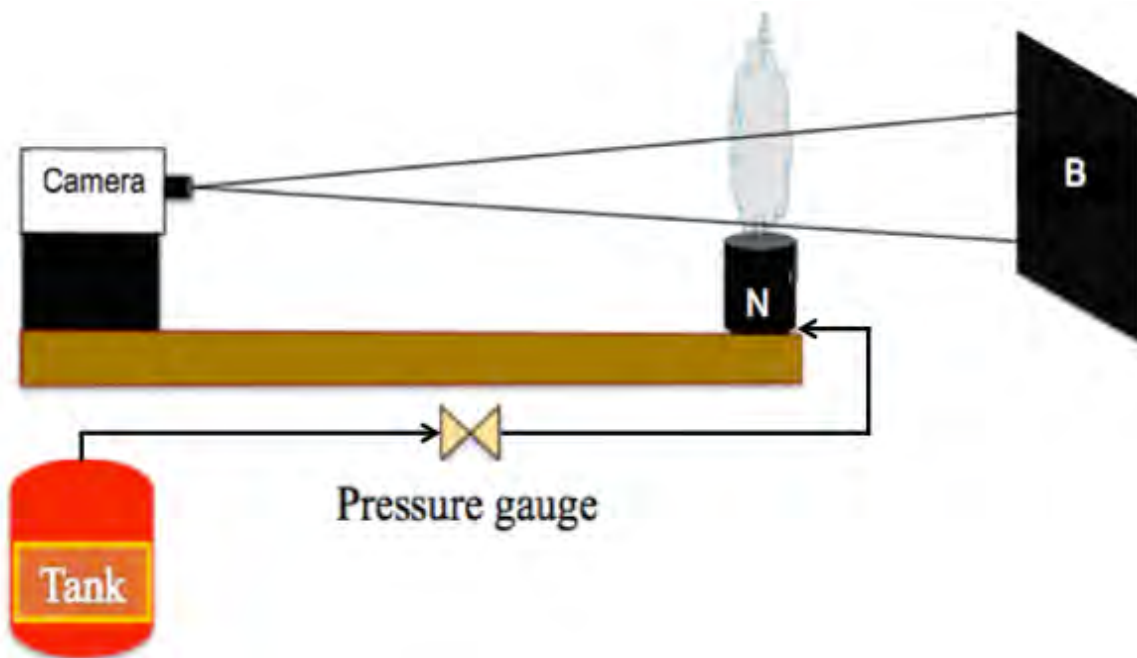


Figure 5.1: The experimental setup for BOS.

The complete experimental setup, illustrating the arrangement of the aforementioned components, is shown in the figure below.



Figure 5.2: Photography of experimental setup.

5.2 Experimental Equipment

This table presents all equipment or tools that are include and used throughout the experiment.

Table 5.1: Experimental equipment.




Equipment	Function
<p>Nozzle</p> 	<ul style="list-style-type: none">❖ The nozzle has exit inner diameter 5.8 mm to deliver the flow field.
<p>Tank of helium gas</p> 	<ul style="list-style-type: none">❖ Feed the nozzle with helium gas by plastic hose.
<p>Pitot tube</p> 	<ul style="list-style-type: none">❖ Determine the pressure for the flow exit

Table 5.1 - continued









Equipment	Function
<p>Camera</p> 	<ul style="list-style-type: none"> ❖ Captures images at high speed.
<p>Lens</p> 	<ul style="list-style-type: none"> ❖ Sets the camera to focus properly for the resolution.
<p>Pressure Gauge</p> 	<ul style="list-style-type: none"> ❖ Controls the flow rate.
<p>Level</p> 	<ul style="list-style-type: none"> ❖ Confirms the configuration of the system is level.

Table 5.1 - continued

Equipment	Function
<p>Spot Light</p> 	<ul style="list-style-type: none"> ❖ Generates uniform light.
<p>Clamp</p> 	<ul style="list-style-type: none"> ❖ Keeps all equipment fixed in place.
<p>Computer</p> 	<ul style="list-style-type: none"> ❖ Records images.
<p>Background</p> 	<ul style="list-style-type: none"> ❖ Visualizes the density gradients between images with and without flow.

5.3 Data Processing

This section presents the procedures that applied to analyze the images from the experiment. This analysis depends on the determinations as follows:

First, the disturbed image to the reference image by image registration, which largely depends on the affine transformation. It is applied to those images to correct any misalignment between their coordinates due to the possible movement or inclination of the camera and other factors throughout the experiment.

Second, the main principle in the BOS technique is to determine the displacement vector field in the background reference image and the corresponding disturbed image. This procedure is executed by using the optical flow method. The optical flow is based on a form typical of the transport equation that used to determine the shift of each pixel in the image plane. Liu and Shen derive the physics-based optical flow equation [21] :

$$\frac{\partial g}{\partial t} + \nabla(gu) = f(x, y, g). \quad (5.3)$$

Where $g = g(I)$ is a function of the normalized image intensity I , $\nabla = \left(\frac{\partial}{\partial x}, \frac{\partial}{\partial y}\right)$, $u = (u, (\Delta x, \Delta y))$ is the velocity vector in the image plane, x and y are the image coordinates. The velocity u multiplied by the unit time t is the displacement $(\Delta x, \Delta y)$.

Finally, the Poisson equation was solved numerically by the applied Gaussian elimination direct method. This method is comparably faster than the iterative method, which is considerably time-consuming. This procedure was used for all 500 images to extract the density gradient data of each image. Furthermore, the turbulence computation was used to study physical characteristics of density fluctuation. The flow chart below demonstrates the main procedures for analyzing images.

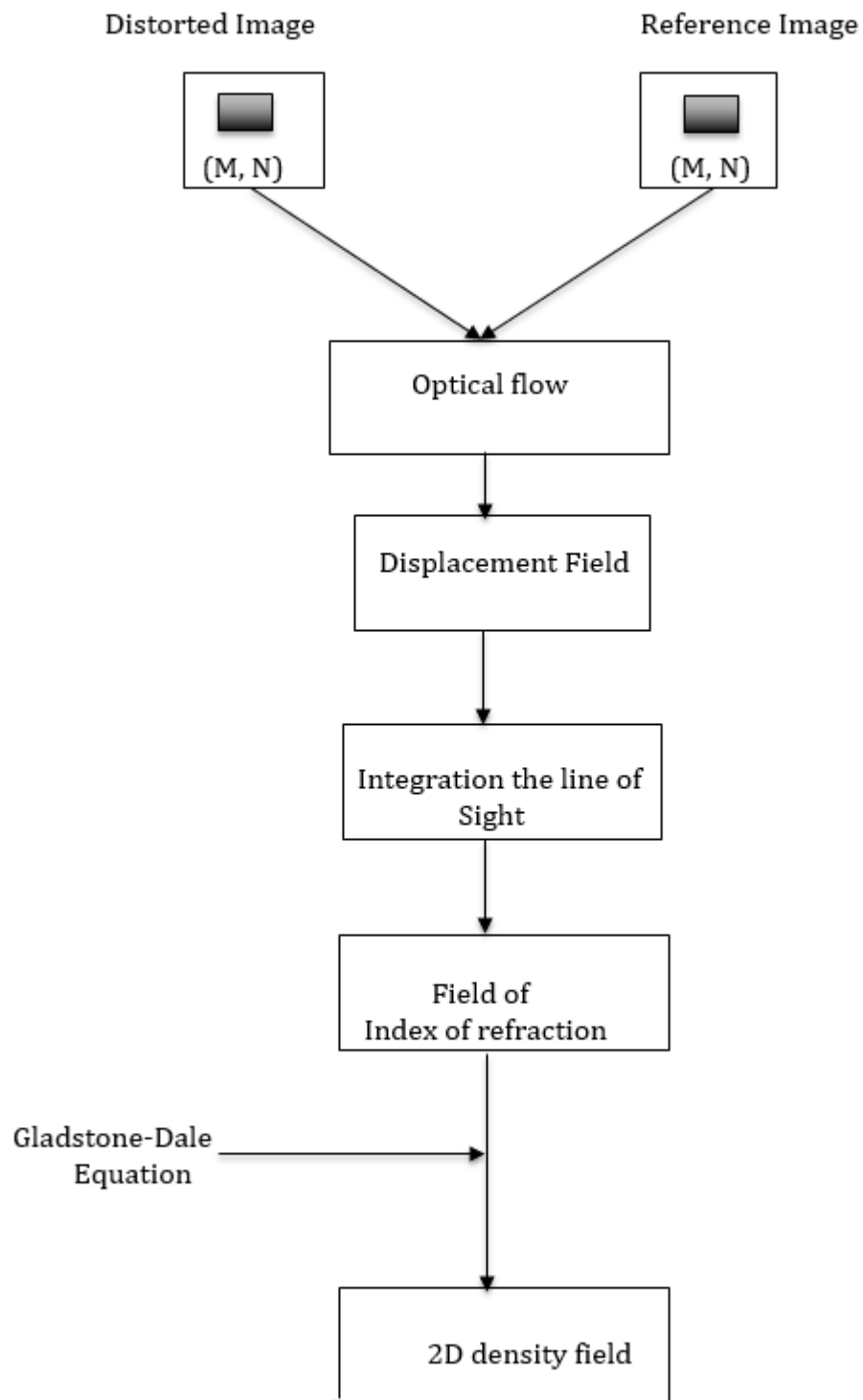


Figure 5.3: Flow chart of the density field calculation with BOS.

CHAPTER 6

RESULTS AND DISCUSSION

This section demonstrates the results of two cases that were done through the experimental work. These results explain the behavior of density variation and effect of changing pressure from low to high on the flow field.

6.1 Low Pressure

This case is executed at helium pressure equal to 0.002 psi and 637.67 of Reynold number, and analyzed using optical flow. Figure 6.1 shows the displacement magnitude fields of sample average for 500 images, each of which contains 1024×1024 vectors. By solving Poisson's equation, Figure 6.2 illustrates the density field regions for density flow of Helium gas through the air, specifically the low density zone above the nozzle. Figure 6.3 gives examples of random images of the density field from the experiment. In addition, Figures 6.4 and 6.5 demonstrate the density profile, and its normalized counterpart, at different elevations. Similarly, Figures 6.6 and 6.7 both illustrates the physical behavior for the density gradient at several specific elevations. The density fluctuation, based on the turbulence calculation, is shown in Figure 6.8.

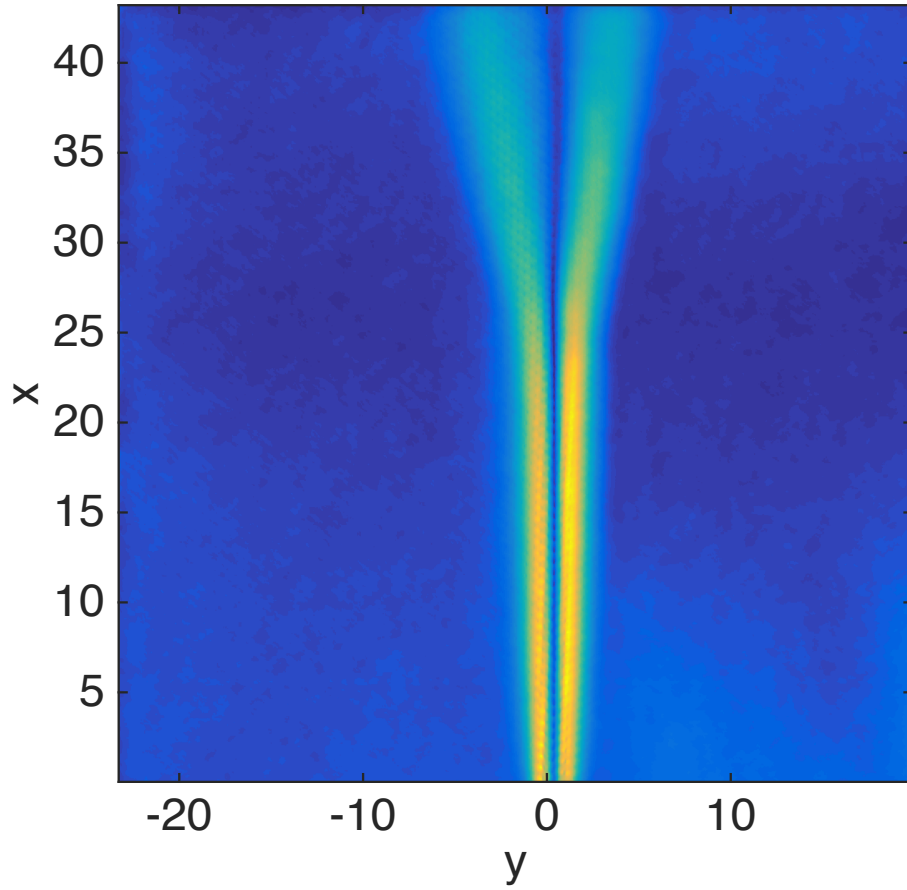


Figure 6.1: The displacement magnitude fields for simple average of 500 images.

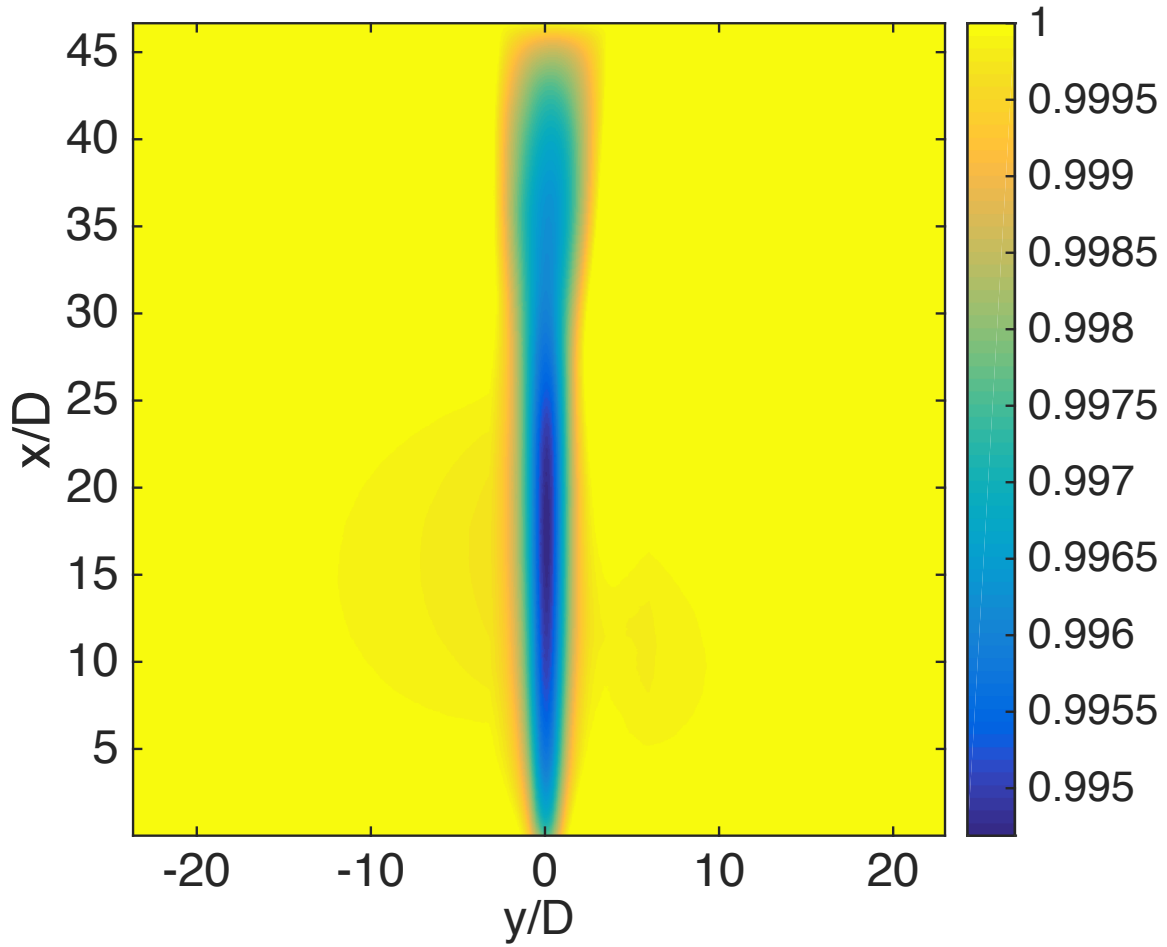


Figure 6.2: Density field for simple average of 500 images at pressure 0.002 psi.

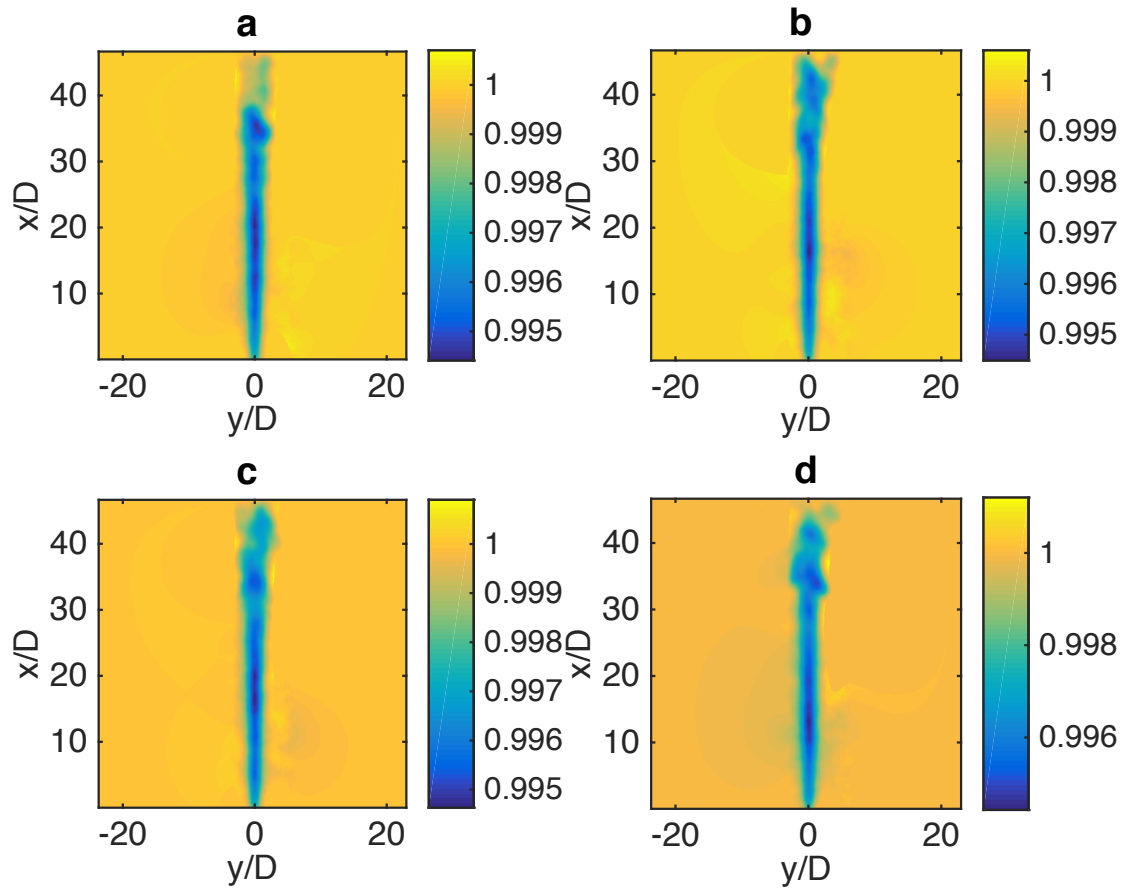


Figure 6.3: Density field of random images. a- image no. 150, b- image no. 250, c- image no. 350, d- image no. 480.

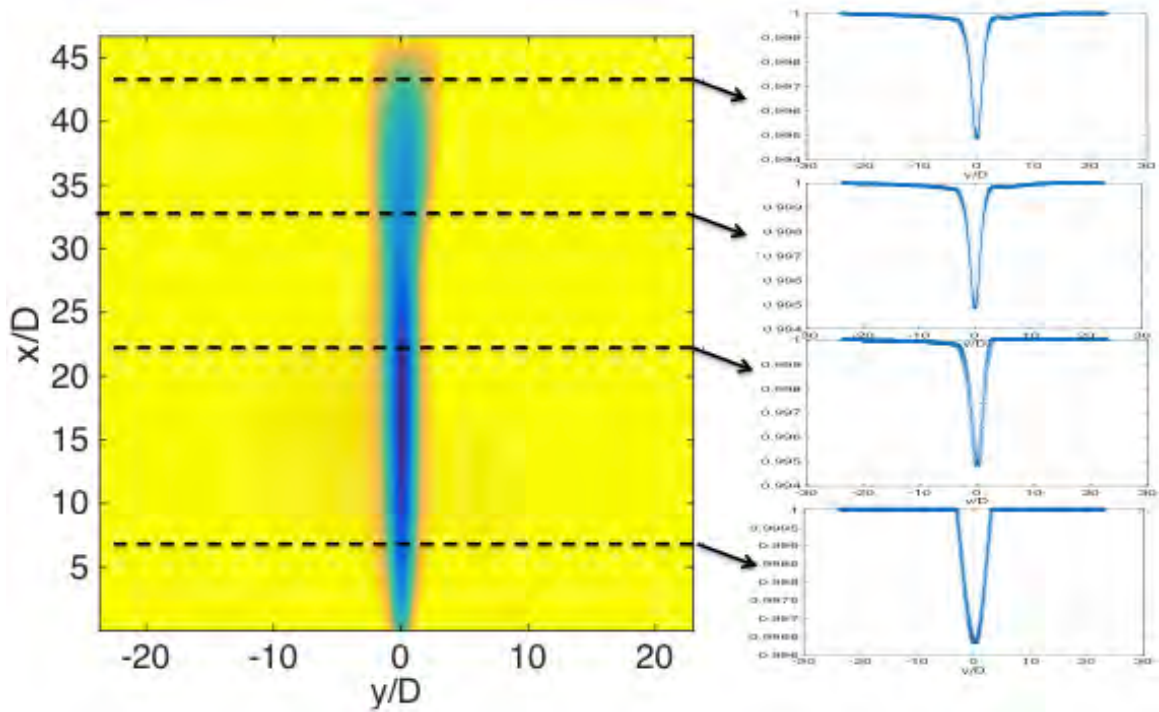


Figure 6.4: Density profile at different elevations.

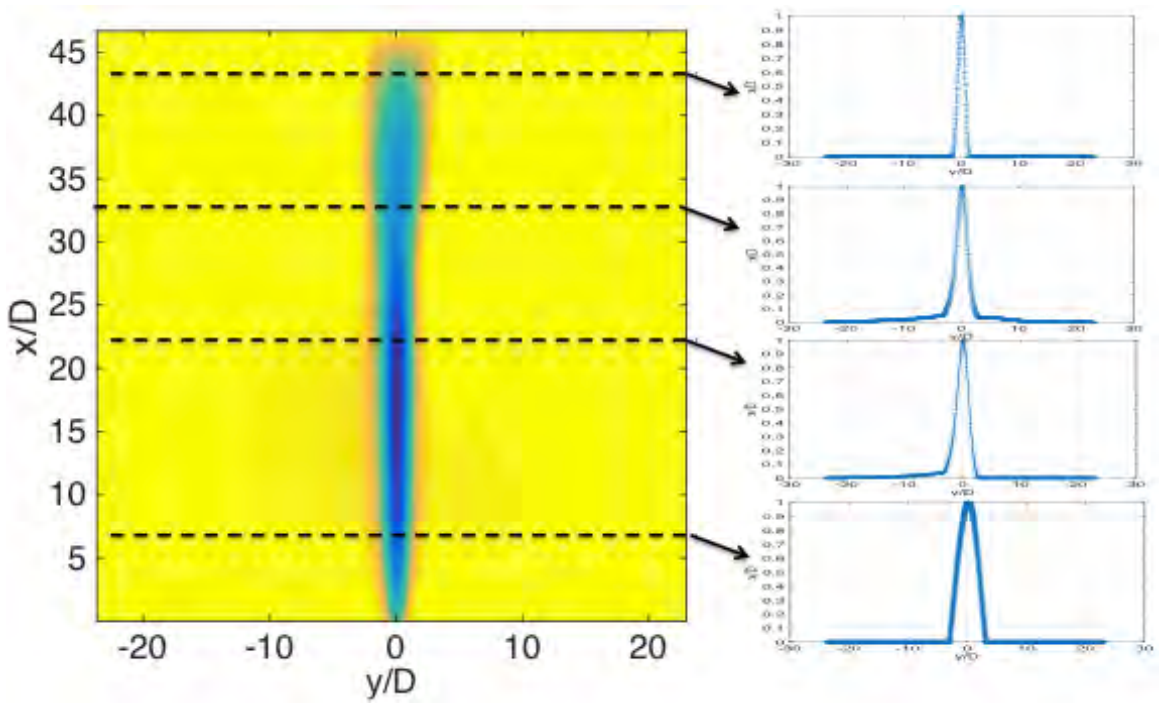


Figure 6.5: Normalizing density profile at different elevations.

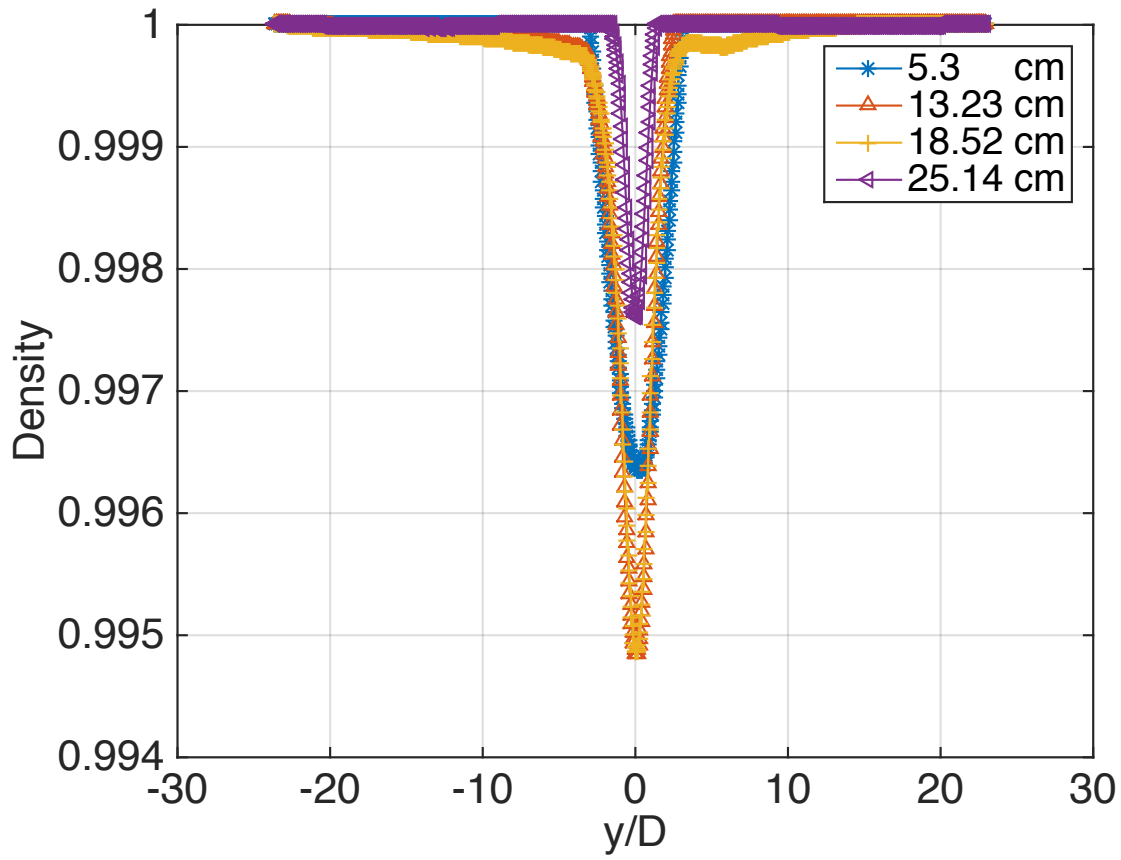


Figure 6.6: Overlapping density profiles at different elevations.

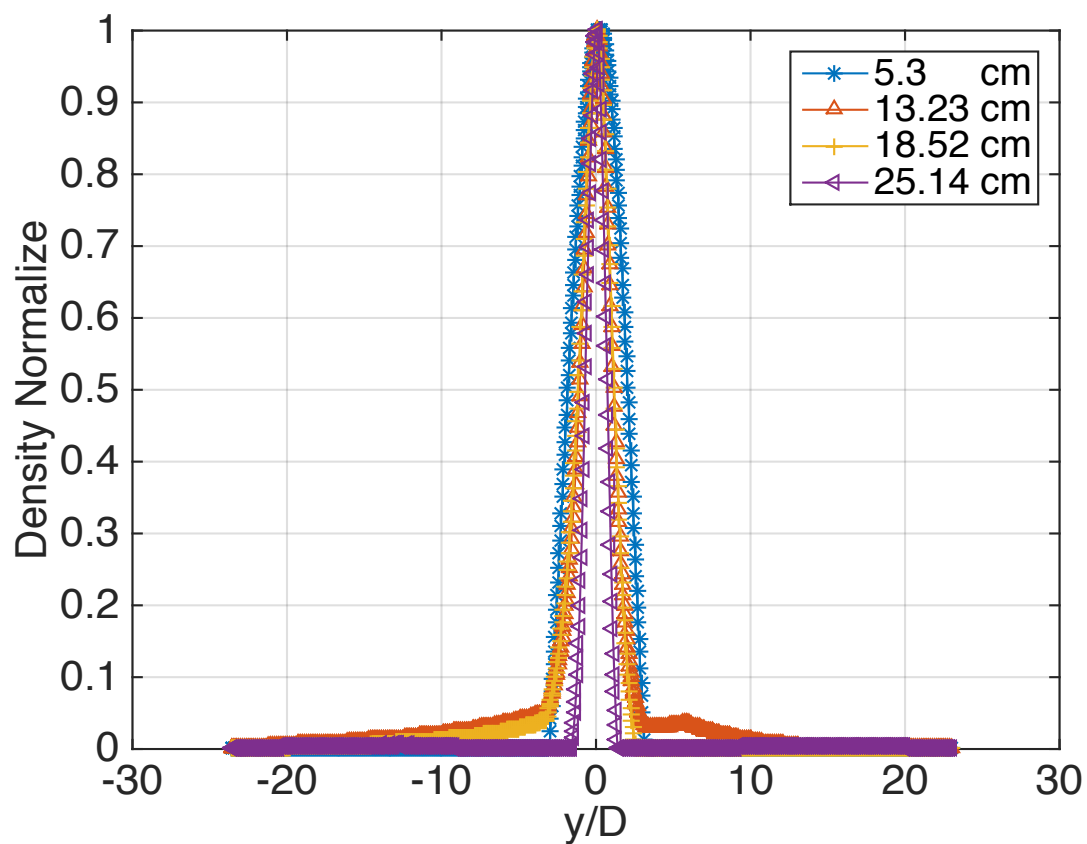


Figure 6.7: Normalized overlapping density profiles at different elevations.

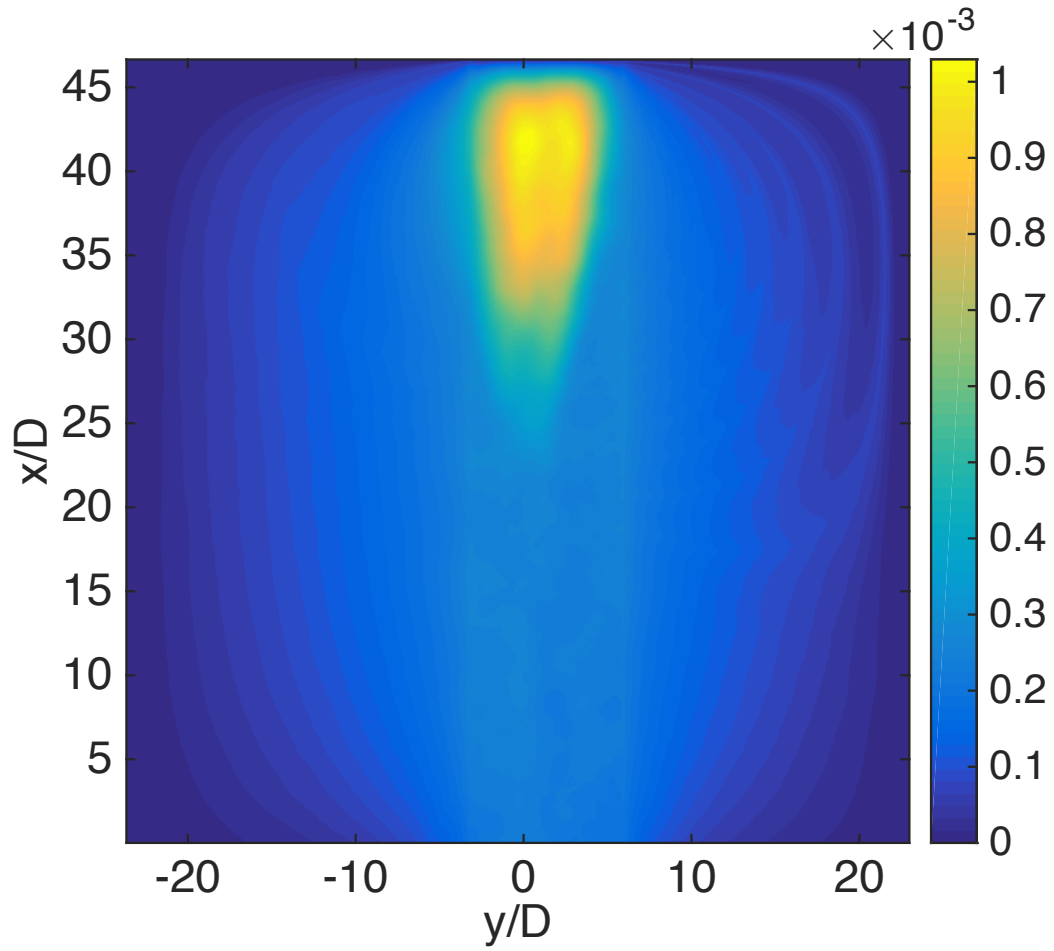


Figure 6.8: Density fluctuation for sample average of 500 images.

6.2 High Pressure

This case is executed at helium pressure equal to 0.005 psi, and analyzed using optical flow. Figure 6.9 shows the average displacement and magnitude fields for 500 images, each of which contains 1024×1024 vectors. By solving Poisson's equation, Figure 6.10 illustrates the density field regions for density flow of Helium gas through the air, specifically the low density zone above the nozzle and the turbulence case is started early due to high pressure and the flow becomes wider. Figure 6.11 gives examples of random images of the density field from the experiment. In addition, Figures 6.12 and 6.13 demonstrate the density profile, and its normalized counterpart, at different elevations. Figure 6.14 illustrates the physical behavior for the density gradient at several specific elevations. The density fluctuation, based on the turbulence calculation, is shown in Figure 6.15.

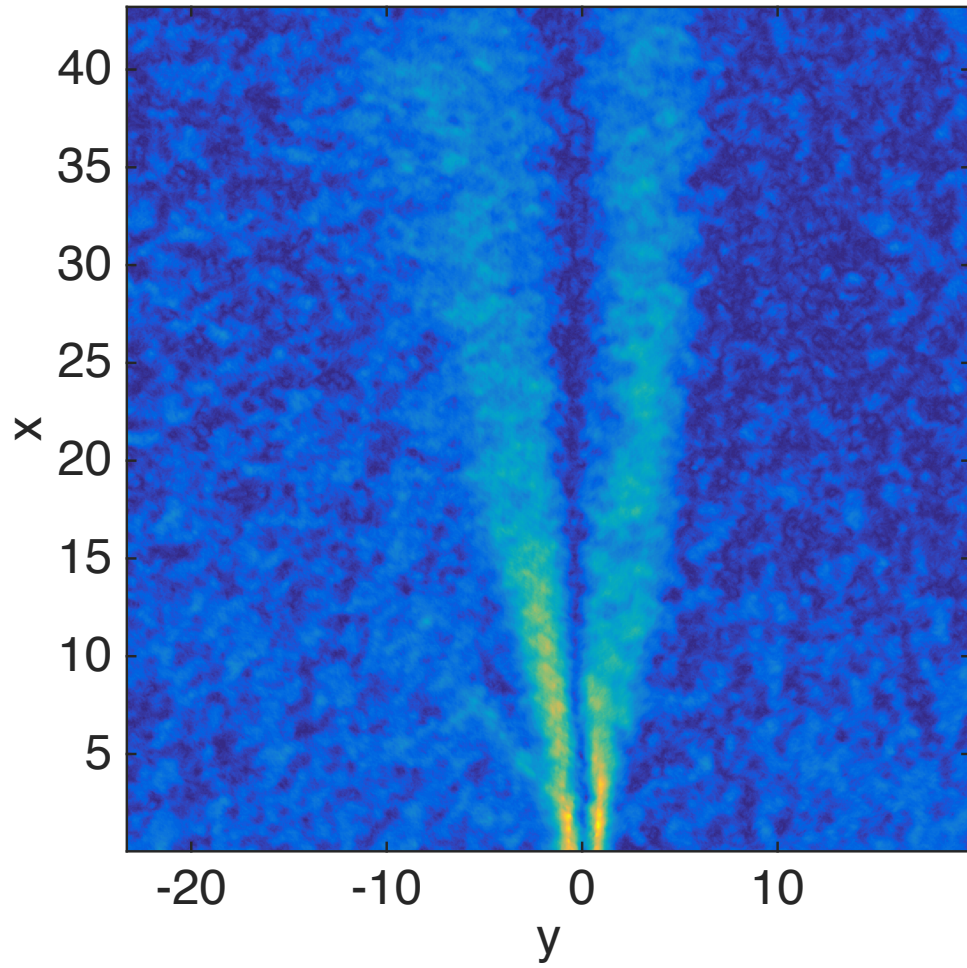


Figure 6.9: The displacement magnitude fields for sample average of 500 images.

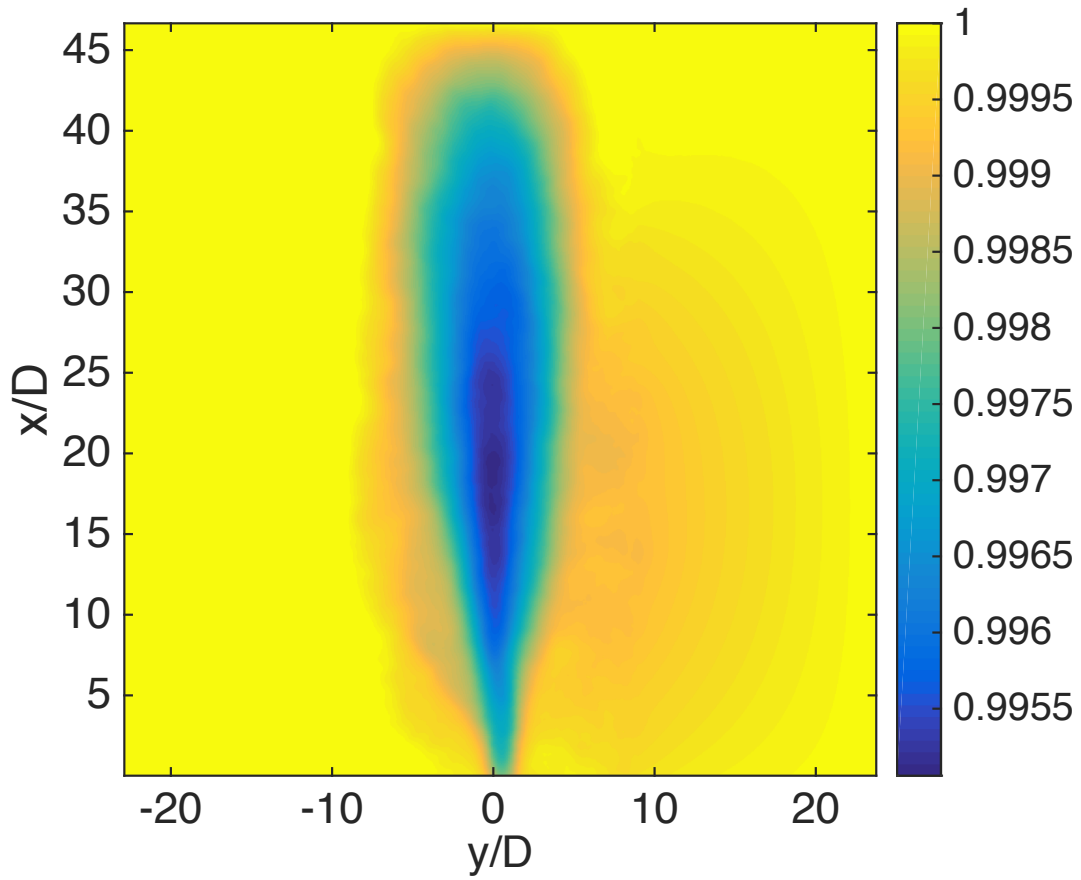


Figure 6.10: Density field for a sample average of 500 images at high pressure 0.005 psi.

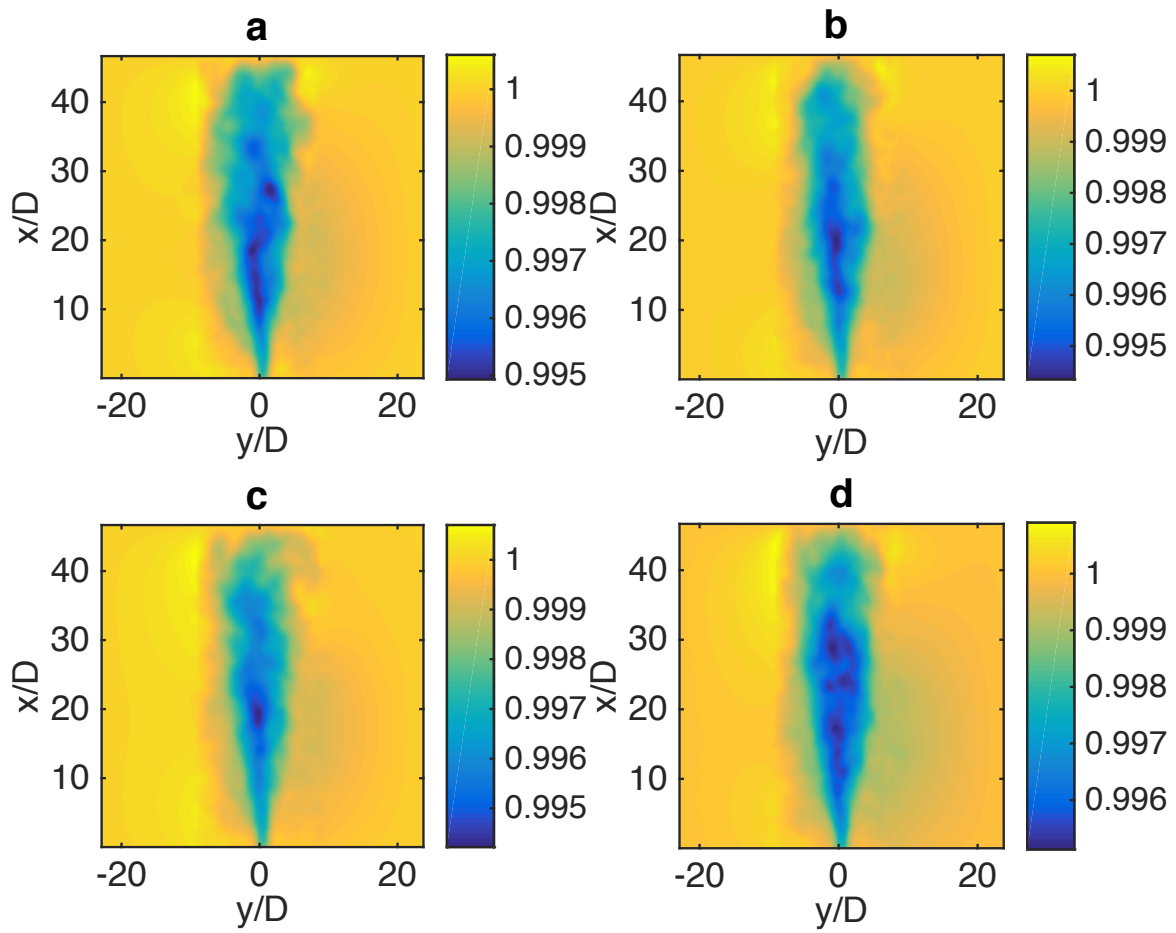
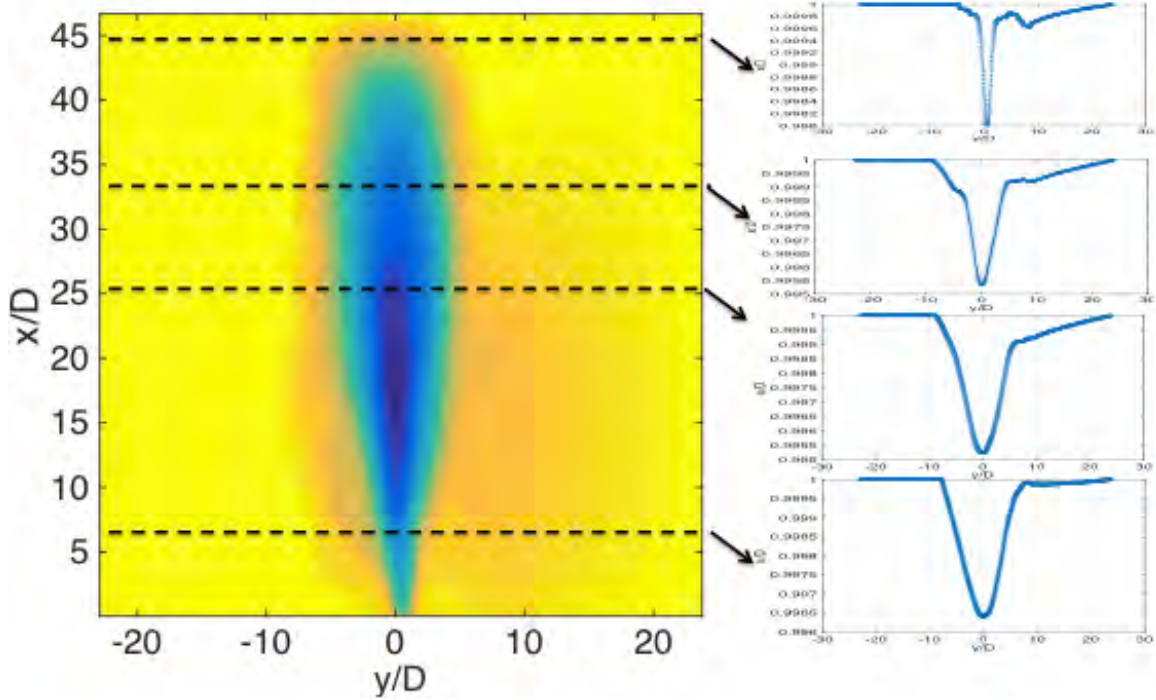
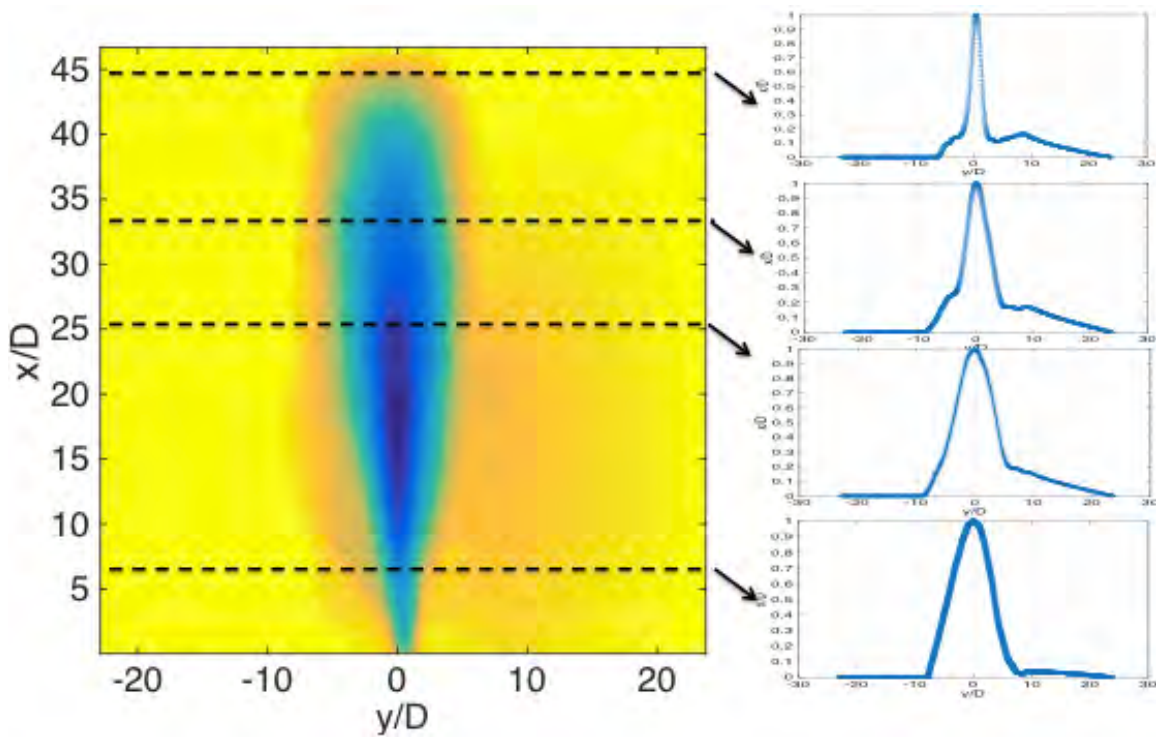


Figure 6.11: Density field of random images. a- image no. 150, b- image no. 250, c- image no. 350, d- image no. 480.



6.12: Density profile for a sample average of 500 images at different elevations.



6.13: Normalizing density profile for a sample average of 500 images at different elevations.

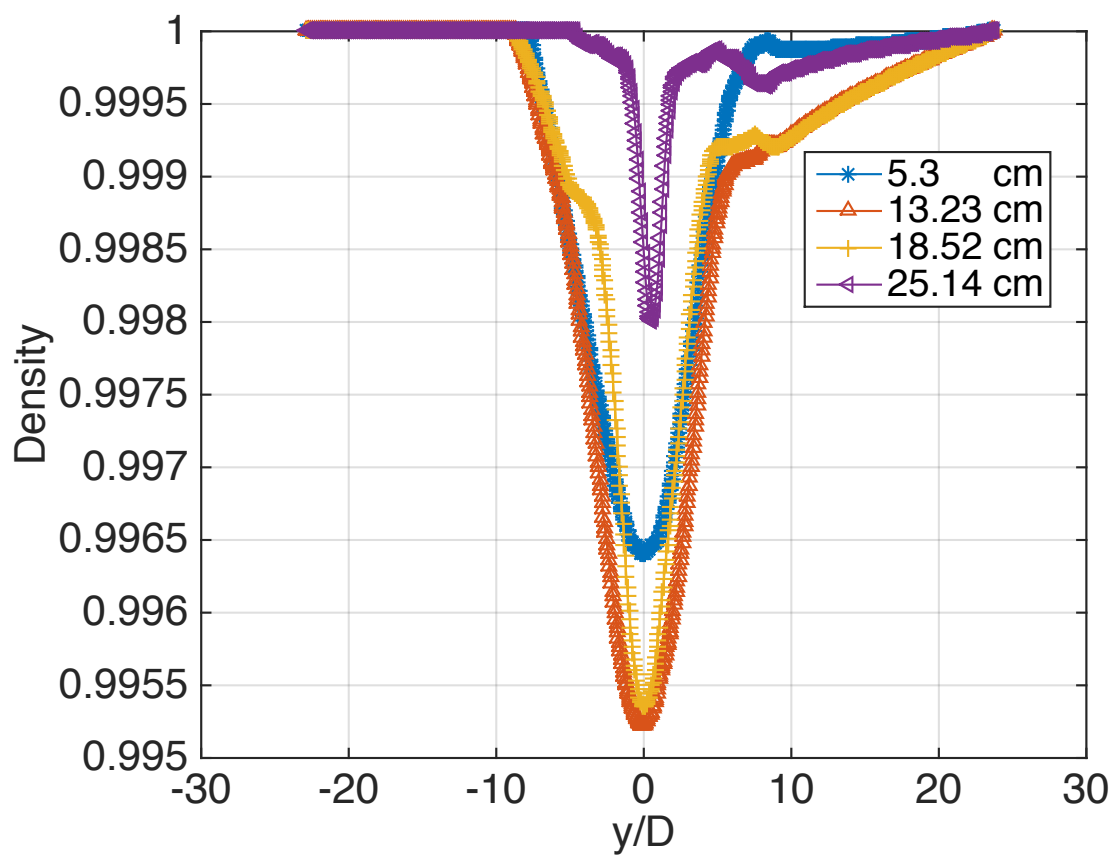


Figure 6.14: Overlapping density profiles of a sample average from 500 images at different elevations.

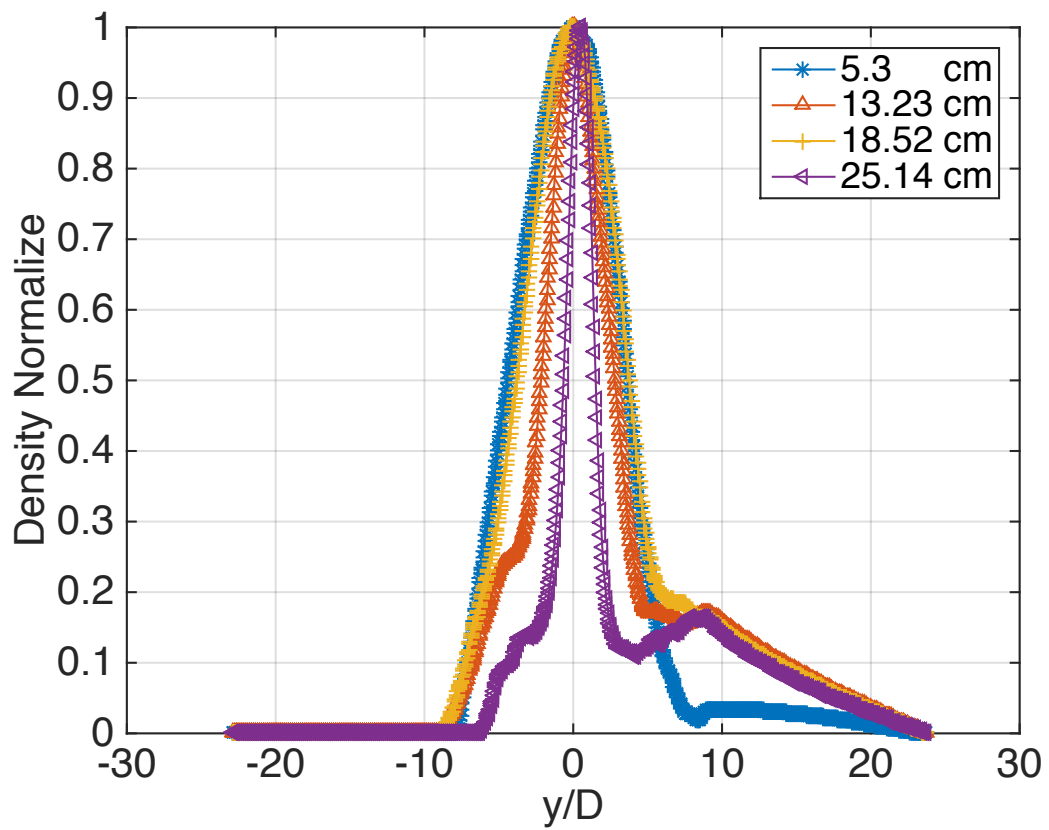


Figure 6.15: Normalized overlapping density profiles for a sample average of 500 images at different elevations.

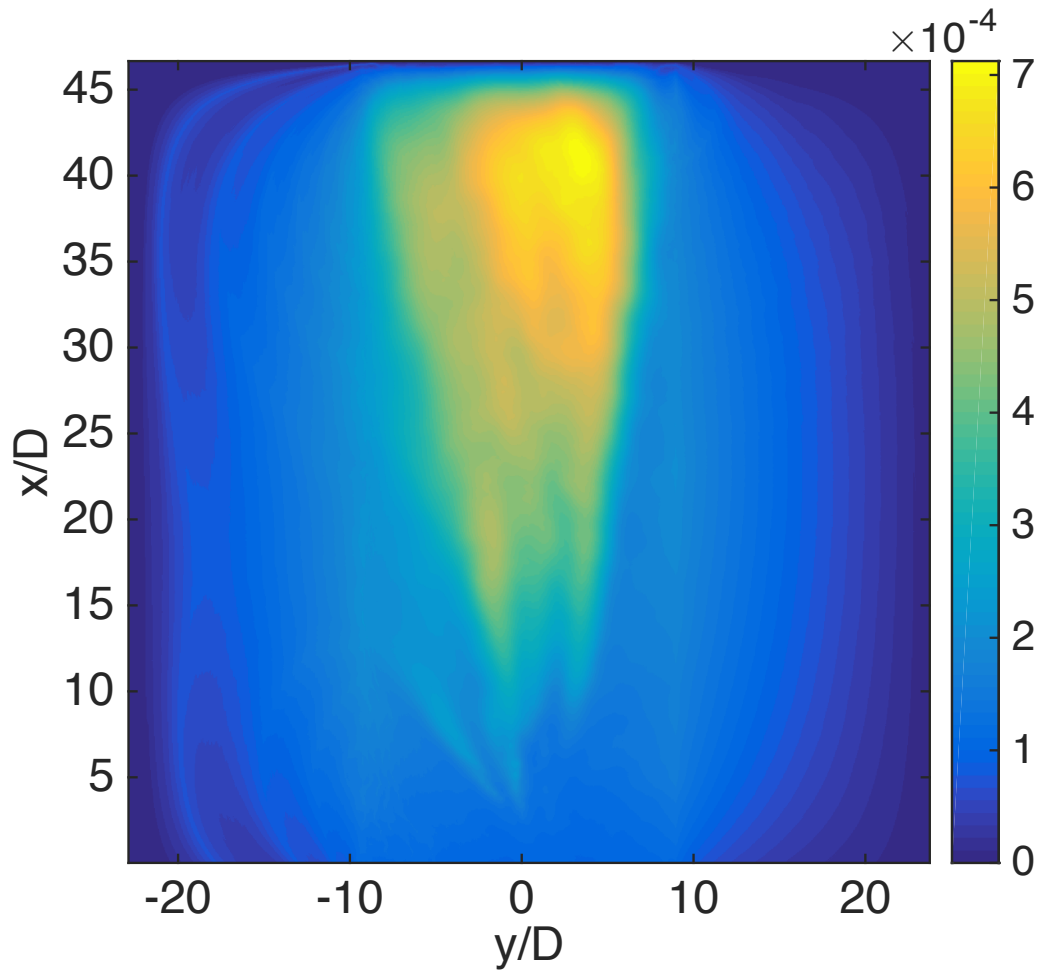


Figure 6.16: Density fluctuation for sample average of 500 images.

CHAPTER 7

CONCLUSION AND FUTURE WORK

7.1 Conclusion

The results presented in this study showed the general possibility to investigate the change of density using optical methods. In BOS measurements of the density gradient for helium gas flow in the ambient air, it was crucial to obtain the displacement vector field. The optical flow method was included into the BOS technique in which the displacement vector field can be obtained from BOS images at the theoretical resolution of one vector per pixel. The results were illustrated two cases of testing, low pressure and high pressure. Furthermore, in the both cases the flow density behavior depended on the pressure level because the flow velocity changes with changing the level of pressure. The flow density field in the low pressure was homogenous flow while in the high pressure was observed random flow at low level above the nozzle exit. The BOS measurements visualized the flow field with high resolution in a simple way.

7.2 Future Work

This study has led to greater understanding of how to visualize the density flow and investigate the behavior of gas flow under the effect of different pressure levels. However, some factors were not considered in this investigations.

Future research would explore the possibility of combining the PIV system with the BOS technique to measure the velocity for helium gas.

REFERENCES

- [1] A. M. M. M. C. F. P. M. T Liu, "Comparison between optical flow and cross-correlation methods for extraction of velocity fields from particle images," *Experiments in Fluids* , vol. 56, no. 8, pp. 1-23, 2015.
- [2] T. T. L. A. J. Smits, "Flow Visualization Techniques and Examples," in *Flow Visualization Techniques and Examples*, London, Imperial College Press, 2012, pp. 227-264.
- [3] W. Merzkirch, *Flow Visualization*, New York: Academic Press, 1987.
- [4] A. P. ., T. M. A.D. Gardner, "Upstream porthole injection in a 2-D scramjet model," *Springer*, pp. 369-375, 2001.
- [5] J. E. Lamar, "Flow-Visualization Techniques Used at High Speed by Configuration Aerodynamics Wind-Tunnel-Test Team," *NASA TM 210848*, 4 2001.
- [6] K. S. G. J. V. E. A. H. J. A. H. B. Leonard M. Weinstein, "VISUALIZATION AND IMAGE PROCESSING OF AIRCRAFT SHOCK WAVE STRUCTURES," *First Pacific Symposium on Flow Visualization and Image Processing*, 1997.
- [7] T. E. K. H. a. A. K. T.J. McIntyre1, "Visualisation and measurement of flow on the inlet of an upstream injected supersonic-combustion ramjet," in *Fourth Australian Conference on Laser Diagnostics in Fluid Mechanics and Combustion*, Australia, 2005.
- [8] M. M. R. R. S. K. P. M. T Liu, "Skin Friction Fields and Surface Dye Patterns on Delta Wings in Water Flows," *Journal of Fluids Engineering* , vol. 137, no. 7, p. 071202, 2015.
- [9] G. Meier, "Computerized background-oriented schlieren," *Experiments in Fluids*, vol. 33, p. 181–187, 2000.
- [10] G. O. H. B. R. S. S.B. Dalziel, "Whole-Field density measurement by 'synthetic schlieren'," *Experimental in Fluids*, vol. 28, pp. 322-335, 2000.
- [11] H. R. G. E. A. M. M. Raffel, "On the applicability of background oriented optical tomography for large scale aerodynamic investigations," *Experiments in Fluids-Springer-Verlag*, vol. 28, pp. 477-481, 2000.
- [12] M. R. H Richard, "Principle and applications of the background oriented schlieren (BOS)

- method," *Measurement Science and technology*, pp. 1576-1585, 16 8 2001.
- [13] G. E. A. M. L. Venkatakrisnan, "Density measurments using the Background Oriented schlieren technique," *Experiments in Fluids*, vol. 37, pp. 237-247, 2004.
- [14] J. L. Sims, "Tables for supersonic flow around right circular cones at zero angle of attack," *NASA Marshall Space Flight Center*, 1964.
- [15] D. R. H. a. J. S. Gaurav Vasudeva, "Non-Intrusive measurement of a density field using the Background Oriented Schlieren(BOS) method," in *Fourth Australian Conference on Laser Diagnostic in Fluid Mechanics and Combustion*, 2005.
- [16] A. w. R. K. a. F. A. L. Venkatakrisnan, "Density Field Measurment of a Supersonic Impinging Jet with Microjet Control," *AIAA Journal*, vol. 49, 2 11 2011.
- [17] A. V. U. Y. Y. P. Nikolay A. Vinnichenko, "Combined study of heat exchange near the liquid–gas interface by means of Background Oriented Schlieren and Infrared Thermal Imaging," *Experimental Thermal and Fluid Science*, vol. 59, p. 238–245, 2013.
- [18] M. K. A. K. J. G. A. L. T. J. N. Kotchourko, "Cocentration measurments in a round hydrogen jet using Background Oriented Schlieren (BOS) technque," *International journal of Hydrojen energy*, 2014.
- [19] Y. T. T. L. M. k. K. Hayasaka, "Measurment of a laser-induced underwater shock wave by the optical-flow-based background- oriented schlieren technique," in *18th International Symposium on the Application pf laser and imaging Techniques to Fluid mechanics*, LISBON, PORTUGAL, 2016.
- [20] M. Raffel, "Bacground-oriented schlieren (BOS) technique," *Experiment fluid*, 6 3 2015.
- [21] L. S. Tianshu Liu, "Fluid flow and optical flow," *Fluid mech*, vol. 614, pp. 253-291, 7 7 2008.
- [22] J. S. Erik Goldhahn, "The background oriented schlieren technique: sensitivity, accuracy, resolution and application to a three-dimensional density field," *Experiment fluid*, pp. 241-249, 10 7 2007.
- [23] J. A. G.-V. a. d. M.-H. Adrian Martinez-Gonzalez, "Temperature and velocity measurment fields of lfuids using a schlieren system," *optical society of America* , vol. 51, 14 2 2012.

APPENDIX A

Numerical Solution

APPENDIX B

Matlab Code

% This code is developed to solve the Poisson equation for BOS Data.

% It is applied for each image and save it automatically.%

clear all;

close all;

tic

numfiles=500;

for k=1:numfiles

 II=strcat('UX',num2str(k),'.mat');

 I=strcat('UY',num2str(k),'.mat');

 ux = dlmread(II);

 uy = dlmread(I);

 ux(isnan(ux))=0;

 uy(isnan(uy))=0;

for i=1:1024

```

for j=1:1024
if i&j<300
ux(i,j)=0;
uy(i,j)=0;
elseif i&j>700
ux(i,j)=0;
uy(i,j)=0;
end
end
end

level_wavelet=0; % 0 = no downsampling, 1 = downsampling by 2, 2 = downsampling by 2^2=4
size_filter=1; % in pixels

[rho,x,y]=density_BOS_fun(ux,uy,level_wavelet,size_filter);
dlmwrite(['roh' num2str(k) '.dat'],rho);
fprintf('Just finished iteration #'%d\n', k)
end

```

```

% This code is developed to all results after saving the data %

%%%%%%%%%%%%%%%%%%%%%%%%%%%%%%%%%%%%%%%%%%%%%%%%%%%%%%%%%%%%%%%%%%%%%%%%

load('Den_avg_H.dat');

load('rms.dat');

load('f_density_avg_s.dat');

load('roh350.dat');

load('roh480.dat');

load('roh250.dat');

load('roh150.dat');

[x,y]=meshgrid(-503:522,1:1026);

X=x./22;

Y=y./22;

for i=1:1026

    for j=1:1026

```

```

if Den_avg_H(i,j)>1
Den_avg_H(i,j)=1;
end
end
end

Den_avg1=Den_avg_H;
DEN=(1-Den_avg1(200,:))/max(1-Den_avg1(200,:));
DEN1=(1-Den_avg1(500,:))/max(1-Den_avg1(500,:));
DEN2=(1-Den_avg1(700,:))/max(1-Den_avg1(700,:));
DEN3=(1-Den_avg1(900,:))/max(1-Den_avg1(900,:));
DEN4=(1-Den_avg1(1000,:))/max(1-Den_avg1(1000,:));

figure (1)
plot(X(1,:),DEN(1:,:), '*-',...
X(1,:),DEN2(1:,:), '^-',...
X(1,:),DEN1(1:,:), '-+',X(1,:),DEN3(1:,:), '<-')
h=xlabel('y/D');
set(h, 'FontSize', 20)
set(gca,'FontSize', 20)
c=ylabel('x/D');
set(c, 'FontSize', 20)
set(gca,'FontSize', 20)
grid on;

figure (2)

```

```
plot(X(1,:),DEN(1,:), '*-', 'linewidth', 2)
```

```
h=xlabel('y/D');
```

```
set(h, 'FontSize', 20)
```

```
set(gca, 'FontSize', 20)
```

```
c=ylabel('x/D');
```

```
set(c, 'FontSize', 20)
```

```
set(gca, 'FontSize', 20); grid on;
```

```
figure (3)
```

```
plot(X(1,:),DEN2(1,:), '^-',
```

```
h=xlabel('y/D');
```

```
set(h, 'FontSize', 20)
```

```
set(gca, 'FontSize', 20)
```

```
c=ylabel('x/D');
```

```
set(c, 'FontSize', 20)
```

```
set(gca, 'FontSize', 20); grid on;
```

```
figure (4)
```

```
plot(X(1,:),DEN1(1,:), '-+')
```

```
h=xlabel('y/D');
```

```
set(h, 'FontSize', 20)
```

```
set(gca, 'FontSize', 20)
```

```
c=ylabel('x/D');
```

```
set(c, 'FontSize', 20)
```

```
set(gca, 'FontSize', 20); grid on;
```

```

figure (5)
plot(X(1,:),DEN3(1,:),'<-')
h=xlabel('y/D');
set(h, 'FontSize', 20)
set(gca,'FontSize', 20)
c=ylabel('x/D');
set(c, 'FontSize', 20)
set(gca,'FontSize', 20);grid on;

% the density field for random images that taken through the test%

figure(6)
subplot(2,2,1)
imagesc(X(1,:),Y(:,1),flipud(roh150(1:950,:)));
h=xlabel('y/D');
set(h, 'FontSize', 15)
set(gca,'FontSize', 15)
c=ylabel('x/D');
set(c, 'FontSize', 15)
set(gca,'FontSize',15)
colorbar
axis image;
set(gca,'YDir','normal');
title('a ');
subplot(2,2,2)

```

```

imagesc(X(1,:),Y(:,1),flipud(roh250(1:950,:)));
h=xlabel('y/D');
set(h, 'FontSize', 15)
set(gca,'FontSize', 15)
c=ylabel('x/D');
set(c, 'FontSize',15)
set(gca,'FontSize', 15)
axis image;
colorbar
set(gca,'YDir','normal');
title('b ');
subplot(2,2,3)
imagesc(X(1,:),Y(:,1),flipud(roh350(1:950,:)));
h=xlabel('y/D');
set(h, 'FontSize', 15)
set(gca,'FontSize',15)
c=ylabel('x/D');
set(c, 'FontSize', 15)
set(gca,'FontSize',15)
axis image;
colorbar
set(gca,'YDir','normal');
title('c ');

```



```

subplot(2,2,4)

imagesc(X(1,:),Y(:,1),flipud(roh480(1:950,:)));

h=xlabel('y/D');

set(h, 'FontSize', 15)

set(gca,'FontSize', 15)

c=ylabel('x/D');

set(c, 'FontSize', 15)

set(gca,'FontSize', 15)

axis image;

colorbar

set(gca,'YDir','normal');

title('d');

% plot the solution for density field average%

figure(7)

set(gcf,'DefaultAxesFontSize',8,'PaperPosition', [0 0 3.5 3.5]),

mesh(x,y,Den_avg1)

figure(8);

imagesc(X(1,:),Y(:,1),flipud(Den_avg_H(1:950,:)));

h=xlabel('y/D');

set(h, 'FontSize', 20)

set(gca,'FontSize', 20)

c=ylabel('x/D');

set(c, 'FontSize', 20)

```

```

set(gca,'FontSize', 20)
ylabel('x/D');
axis image;
set(gca,'YDir','normal');
skip=15;
% plot the density profile at different elevations %
figure(9)
plot(X(1,:),Den_avg1(200,:), '*-',...
X(1,:),Den_avg1(500,:), '^-',...
X(1,:),Den_avg1(700,:), '-+',...
X(1,:),Den_avg1(950,:), '<-');grid on;
h=xlabel('y/D');
set(h, 'FontSize', 20)
set(gca,'FontSize', 20)
c=ylabel('x/D');
set(c, 'FontSize', 20)
set(gca,'FontSize', 20)
figure (10)
plot(X(1,:),Den_avg1(200,:), '*-')
h=xlabel('y/D');
set(h, 'FontSize', 20)
set(gca,'FontSize', 20)
c=ylabel('x/D');

```

```

set(c, 'FontSize', 20)
set(gca,'FontSize', 20);grid on
figure (11)
plot( X(1,:),Den_avg1(500,:),'^-')
h=xlabel('y/D');
set(h, 'FontSize', 20)
set(gca,'FontSize', 20)
c=ylabel('x/D');
set(c, 'FontSize', 20)
set(gca,'FontSize', 20);grid on
figure (12)
plot(X(1,:),Den_avg1(700,:),'-+')
h=xlabel('y/D');
set(h, 'FontSize', 20)
set(gca,'FontSize', 20)
c=ylabel('x/D');
set(c, 'FontSize', 20)
set(gca,'FontSize', 20);grid on
figure (13)
plot(X(1,:),Den_avg1(950,:),'<-')
h=xlabel('y/D');
set(h, 'FontSize', 20)
set(gca,'FontSize', 20)

```

```

c=ylabel('x/D');
set(c, 'FontSize', 20)
set(gca,'FontSize', 20);grid on
[m,n]=size(Den_avg1);
% plot the trend for density gradient%
figure (14)
plot(X(1,1:end),Den_avg1(round(m/2),:),'-', 'linewidth',2);
h=xlabel('y/D');
set(h, 'FontSize', 20)
set(gca,'FontSize', 20)
c=ylabel('x/D');
set(c, 'FontSize', 20)
set(gca,'FontSize', 20)
% title('Density profile')
grid;
% plot the root mean square
figure (15)
set(gcf,'DefaultAxesFontSize',8,'PaperPosition', [0 0 3.5 3.5]),
mesh(x,y,rms)
figure(16);
imagesc(X(1,:),Y(:,1),flipud(rms(1:950,:)));
h=xlabel('y/D');
set(h, 'FontSize', 20)

```

```
set(gca,'FontSize', 20)
c=ylabel('x/D');
set(c, 'FontSize', 20)
set(gca,'FontSize', 20)
axis image;
set(gca,'YDir','normal');
% title('Density fluctuation Field');
colorbar;
```